NASA TECHNICAL NOTE

NASA TN D-6831

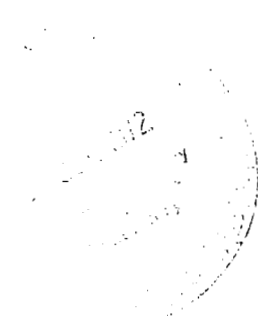# EXPERIMENTAL INVESTIGATION OF STABILITY AND STALL FLUTTER OF A FREE-FLOATING WING V/STOL MODEL

by Robert A. Ormiston

Ames Research Center

and

U.S. Army Air Mobility R&D Laboratory
Moffett Field, Calif. 94035

1. Report No. NASA TN D-6831	2. Government Accession No.	3. Recipient's Catalog No.
4. Title and Subtitle EXPERIMENTAL INVESTIGATION OF STABILITY AND STALL FLUTTER OF A FREE–FLOATING WING V/STOL MODEL		5. Report Date June 1972
		6. Performing Organization Code
7. Author(s) Robert A. Ormiston		8. Performing Organization Report No. A-4088
		10. Work Unit No. 760-76-03-06
9. Performing Organization Name and Address NASA Ames Research Center and U. S. Army Air Mobility R & D Laboratory Moffett Field, Calif., 94035		11. Contract or Grant No.
		13. Type of Report and Period Covered Technical Note
12. Sponsoring Agency Name and Address National Aeronautics and Space Administration Washington, D. C., 20546		14. Sponsoring Agency Code

15. Supplementary Notes

Edited by NASA Ames Research Center

16. Abstract

An experimental investigation was made of the static and dynamic stability characteristics of a one-fourth scale model of a tilt-propeller free-wing V/STOL aircraft. The effects of wing pivot location, wing chord, trailing-edge angle, propeller tilt angle, and thrust were studied, and a limited evaluation was made of high-lift devices. A dynamically similar wing was used to measure frequency and damping ratio from transient response data in the linear aerodynamic regime and the results were compared to quasi-steady and unsteady aerodynamic theory. It was found that at high trim angles of attack, in the nonlinear aerodynamic regime, stall flutter oscillations occurred with typical amplitudes ranging from 15° to 20°. Wing control tab deflection was effective in initiating and terminating stall flutter but variations in configuration or operating conditions did not greatly influence the occurrence or characteristics of the oscillations.

17. Key Words (Suggested by Author(s)) V/STOL tilt-propeller V/STOL aircraft Free-floating wing Stall flutter Gust alleviation Wing-slipstream interaction	18. Distribution Statement Unclassified – Unlimited

19. Security Classif. (of this report) Unclassified	20. Security Classif. (of this page) Unclassified	21. No. of Pages 45	22. Price* $3.00

SYMBOLS

a   distance of airfoil semichord point ahead of pivot axis as fraction of semichord, $2\bar{x}_o - 1$

A_p propeller disc area, πR^2, m²

b   airfoil semichord, $\frac{c}{2}$, m

c   wing chord, m

c_t wing control tab chord, m

C(k)   Theodorsen function $C(k) = F(k) + iG(k)$

C_L lift coefficient, $\frac{L}{qS}$

C_m pitching-moment coefficient about wing pivot, $\frac{M}{qS}$, positive nose up

$\left(\frac{\partial C_L}{\partial \alpha}\right)_\delta$ wing lift curve slope, tab fixed, per rad

$\left(\frac{\partial C_L}{\partial \delta}\right)_\alpha$ wing tab lift, α constant, per rad

$\left(\frac{\partial C_m}{\partial \alpha}\right)_\delta$ wing angle-of-attack stability, tab fixed, per rad

$\left(\frac{\partial C_m}{\partial \delta}\right)_\alpha$ wing tab control power, α constant, per rad

$\left(\frac{dC_m}{dC_L}\right)_\delta$ wing static stability

$\left(\frac{d\alpha}{d\delta}\right)_{free}$ wing static floating response

e   ratio of three-dimensional wing lift curve slope to two-dimensional airfoil lift curve slope

F(k)   real part of Theodorsen function

$G(k)$	imaginary part of Theodorsen function
i	$\sqrt{-1}$
I	wing inertia per unit span about pivot axis, kg m
$\bar{I}$	wing relative mass parameter, $\dfrac{8I}{\rho c^4}$
k	reduced frequency, $\dfrac{\omega c}{2U}$
M_{aero}	wing pitching moment per unit span, N
q	dynamic pressure, $\dfrac{\rho U^2}{2}$, N/m²
q_s	slipstream dynamic pressure, q + $\dfrac{T}{A_p}$, N/m²
R	propeller radius, m
Re	Reynolds number, $\dfrac{Uc}{\nu}$
S	wing area, m²
t	time, sec
t_p	elapsed time to first transient overshoot peak, sec
t^*	time constant, $\dfrac{b}{U}$, sec
T	propeller thrust, N
T_c''	propeller thrust coefficient, $\dfrac{T}{q_s A_p}$
U	free-stream velocity, m/sec
x_o	wing pivot axis measured from leading edge, m
x_{ac}	wing aerodynamic center location, m
$\bar{x}_{ac} - \bar{x}_o$	static margin
α	wing angle of attack, deg
α_d	wing angle-of-attack deviation from trim condition, deg (fig. 8)
α_p	propeller shaft angle of attack relative to free stream, deg

iv

$\Delta\alpha$ wing angle overshoot for transient response, deg

$\delta_{1,2,3}$ wing control tab deflection angle, positive trailing edge down, deg, spanwise segment numbers 1, 2, 3 defined in figure 1

ζ damping ratio of wing transient response

η damping of wing motion, sec^{-1}

λ $\eta + i\omega$, sec^{-1}

Λ scale factor, $\dfrac{c_{\text{model}}}{c_{\text{full scale}}}$

ν kinematic viscosity, m^2/sec

ρ air density, kg/m^3

ϕ_{TE} trailing-edge angle, deg (fig. 3)

ω wing damped natural frequency, rad/sec

ω_n wing natural frequency, rad/sec

Superscripts

$(\,\dot{}\,),(\,\ddot{}\,)$ derivatives with respect to time, $\dfrac{d}{dt}$, $\dfrac{d^2}{dt^2}$

$(\,\bar{}\,)$ made dimensionless by c or t^* $\left(\text{i.e., } \bar{x}_o = \dfrac{x_o}{c}, \bar{t} = \dfrac{t}{t^*}\right)$

Subscripts

LE   leading edge

n   nacelle contribution

w   wing contribution

EXPERIMENTAL INVESTIGATION OF STABILITY AND

STALL FLUTTER OF A FREE—FLOATING

WING V/STOL MODEL

Robert A. Ormiston

Ames Research Center
and
U.S. Army Air Mobility Research and Development Laboratory

SUMMARY

An experimental investigation was made of the static and dynamic stability characteristics of a one-fourth scale model of a tilt-propeller free-wing V/STOL aircraft. The effects of wing pivot location, wing chord, trailing-edge angle, propeller tilt angle, and thrust were studied, and a limited evaluation was made of high-lift devices. A dynamically similar wing was used to measure frequency and damping ratio from transient response data in the linear aerodynamic regime and the results were compared to quasi-steady and unsteady aerodynamic theory. It was found that at high trim angles of attack, in the nonlinear aerodynamic regime, stall flutter oscillations occurred with typical amplitudes ranging from 15° to 20°. Wing control tab deflection was effective in initiating and terminating stall flutter but variations in configuration or operating conditions did not greatly influence the occurrence or characteristics of the oscillations.

INTRODUCTION

Freely pivoted airfoils can be used in a wide variety of flight vehicle applications. One potential benefit is the reduction of aircraft response to atmospheric turbulence, or gust alleviation. This is achieved by the rapid dynamic response of a floating airfoil to turbulence-induced angle-of-attack disturbances. Analytical results of reference 1 recently confirmed this aspect of floating wing performance. Another benefit, particularly true in propeller driven V/STOL aircraft, is the possible reduction in adverse wing-slipstream aerodynamic interactions in the hover- and transition-flight regimes. This benefit results because the wing can freely pivot in response to changes in slipstream direction under differing flight conditions.

For practical application to V/STOL configurations, the static and dynamic stability characteristics of the free wing must be known. At low wing angles of attack, and without the influence of the slipstream, these characteristics can be predicted with linear aerodynamic theory. However, experimental techniques are needed to investigate operation within a slipstream or at angles of attack near stall.

Particularly significant for the free wing are possible self-excited, or undamped limit cycle wing oscillations. Experimental measurements (refs. 2 and 3) of the aerodynamic damping moments

of airfoils harmonically oscillated in pitch at high mean angles of attack (in the stall region) have shown that negative damping can occur. For a free-floating airfoil restrained only by aerodynamic forces (weathervane stability), negative damping can lead to stall flutter at high angles of attack. This condition if present could be induced by transient pitch overshoots from control inputs or by gust responses when the wing is trimmed at a high angle of attack. Experiments were conducted to investigate this possibility, using a free-wing model of a representative V/STOL configuration.

Static aerodynamic characteristics of the model were measured in addition to dynamic stability and stall flutter characteristics. These measurements delineate the effects of wing-slipstream interaction on the wing static floating response characteristics and provide baseline static stability data for use in predicting dynamic response in the linear aerodynamic regime. Parameters such as pivot location, airfoil trailing-edge angle, and tab control power, are considered relative to static stability and control of the free wing. Preliminary static test results using the present model were reported in reference 4.

Tests were performed by the 7– by 10–foot wind tunnel at the Ames Directorate, U.S. Army Air Mobility Research and Development Laboratory at Moffett Field, California.

PARAMETER TRADEOFFS FOR FREE–WING DESIGN

The relevant design considerations for free-wing aircraft stem primarily from two mutually conflicting requirements: good gust alleviation, and low-speed, high-lift performance. The conflict is best understood in terms of the opposing requirement for wing static stability. In the first case, good gust alleviation performance is dependent on a high value of the wing pitching natural frequency, which is proportional to wing static stability, dC_m/dC_L. The frequency must be near the highest frequency present in the atmospheric turbulence spectrum, for the wing pitching motion to effectively compensate for gust angle-of-attack perturbations (ref. 1).

On the other hand, the high-lift performance of the free wing is seriously affected by the requirement for pitching equilibrium. As a result, conventional trailing-edge flaps cannot be used since they cause large negative pitching moments. In fact, the trailing-edge control tab used to trim the free wing acts as a flap but in the opposite direction. The resulting lift of the deflected tab therefore opposes the lift of the wing and becomes *adverse lift*. The magnitude of this *adverse lift* is directly proportional to the static stability of the wing because of the required pitching-moment equilibrium.

Accordingly, a major design consideration for a free-wing aircraft is the compromise between the potential gust alleviation performance and the high-lift capability of the wing for low-speed flight conditions.

A secondary effect on wing-pitching frequency and gust alleviation is the static mass balance and inertia properties of the wing. This introduces additional parameters, such as static margin and aerodynamic center, because static mass balancing of the wing about the pivot axis increases the inertia of the wing and reduces its pitching frequency. Any means of shifting the pivot axis rearward, closer to the chordwise mass center of the unbalanced wing structure, minimizes the increase in inertia. The compromise choice of wing static stability, dC_m/dC_L, partially specifies the

2

pivot axis location, since static stability is equivalent to the wing static margin, $\bar{x}_{ac} - \bar{x}_0$. The only other parameter controlling the pivot location then is the aerodynamic center of location, $\bar{x}_{ac}$. Therefore, for a given level of wing static stability, the pivot can be placed farther rearward, the static mass balance reduced, and the pitching inertia minimized for an airfoil having a rearward location of its aerodynamic center. One way of achieving this is by decreasing the airfoil trailing-edge angle.

These design considerations are presented to illustrate the special significance for free-wing aircraft of the static stability parameters discussed in the following results.

MODEL AND TEST PROCEDURE

Model

The general arrangement of the model employed in the experimental investigation of stability and stall flutter is shown in figure 1. The model is a one-fourth scale version of a four seat, light observation, tilt-propeller V/STOL aircraft with approximately a 6.3-meter wingspan. The half-span model consists of a fuselage, a wing, and a single propeller and nacelle, mounted on a fixed ground plane, 0.254 meter above the tunnel floor. Figure 2 shows the model installed in the tunnel.
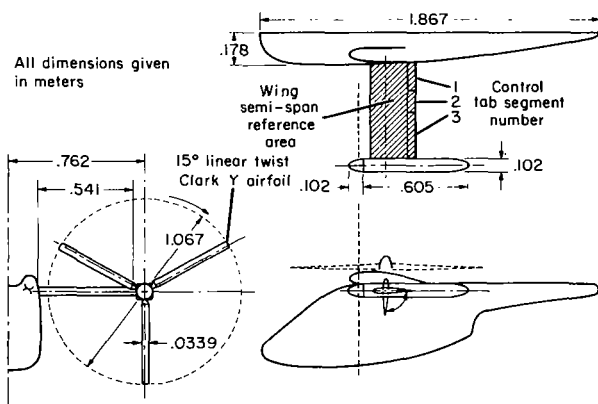

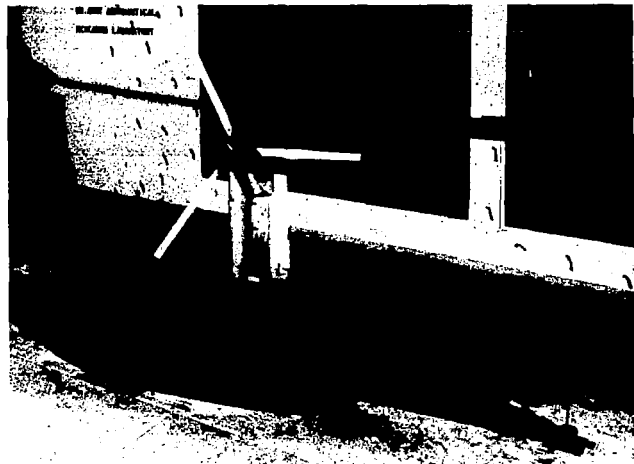Figure 1.- General arrangement of wind-tunnel model.

Figure 2.- Model installed in wind tunnel with static wing.

The propeller and nacelle containing a 20-horsepower electric motor are mounted at the end of a cylindrical wing spar anchored within the fuselage. The wing spar passes through the free-floating wing structure and acts as the pivot for the wing. Bearings at the root and tip of the wing, adjacent to the fuselage and nacelle, respectively, minimize friction between the free-floating wing structure and the fixed wing spar. For the fixed-wing tests, the wing can be mechanically locked to the wing spar.

The propeller and nacelle can be rotated with respect to the fuselage to represent V/STOL transition flight conditions. The propeller (1.067 m diameter) is equipped with three blades of

3

constant chord (0.0339 m). The airfoil section is a Clark Y, 14 percent thick, and the blades have $15°$ linear twist. The pitch angle for all tests was $6°$ at the 0.75 R location.

The model was tested with two different wings, the first one constructed of solid aluminum for static testing. For dynamic tests, a lightweight, wood-veneer covered, plastic-foam wing was used. These are referred to as the static and dynamic wings, respectively. The wing airfoil section is a modified NACA $63_2A_{(015)}-219$ with a reflex camber mean line. The solid aluminum static wing could be tested with leading- and trailing-edge high-lift devices. Profiles and a table of ordinates are given in figure 3.

The conditions necessary for dynamic similarity of the wing are as follows. The wing equation of motion in pitch given in appendix A can be written in terms of dimensionless time: $\bar{t} = t/t^*$, where $t^* = b/U$. When this is done, the equation is identical for wings of any size, if the relative mass parameter, $\bar{I}$, and the reduced frequency, k, are held constant. This ensures that the model is correctly scaled for both inertia and unsteady aerodynamic effects. If a linear scale factor Λ is defined as

Airfoil $63_2A_{(015)}-219$ Mod.			
x_u/c	y_u/c	x_L/c	y_L/c
0	0	0	0
0.002	0.016	0.008	-0.014
.004	.020	.011	- .016
.009	.026	.016	- .021
.021	.037	.029	- .028
.045	.053	.055	- .039
.070	.065	.080	- .046
.095	.075	.105	- .052
.146	.090	.154	- .061
.197	.100	.203	- .067
.248	.108	.252	- .072
.300	.112	.300	- .075
.352	.113	.348	- .077
.403	.110	.397	- .078
.454	.105	.446	- .077
.504	.098	.496	- .075
.555	.090	.545	- .072
.606	.080	.594	- .067
.656	.079	.644	- .062
.706	.058	.694	- .055
.756	.046	.744	- .048
.805	.035	.795	- .040
.855	.026	.845	- .030
.903	.017	.897	- .021
.952	.009	.949	- .011
1.000	.000	1.000	- .000

Figure 3.- Airfoil sections.

$$\Lambda \equiv \frac{c_{model}}{c_{full\ scale}} \qquad (1)$$

then for dynamic similarity

$$\bar{I}_{model} = \bar{I}_{full\ scale} \qquad (2)$$

or

$$\frac{I_m}{\rho_m c_m^4} = \frac{I_{fs}}{\rho_{fs} c_{fs}^4} \qquad (3)$$

and

$$I_m = \left(\frac{\rho_m}{\rho_{fs}}\right) \Lambda^4 I_{fs} \qquad (4)$$

4

If atmospheric density is equal, the wing inertia per unit span for the model is equal to the fourth power of the scale factor times the inertia per unit span of the full scale wing. (The total inertia will then vary with Λ^5.) For comparison purposes, the wing inertia for the full scale design, the static wing, and the dynamic wing are 5.65, 0.040, and 0.00745 kg m^2, respectively.

Since the dynamic scaling is based on dimensionless time, model frequencies are converted to full scale values according to the formula

$$\omega_{fs} = \Lambda \frac{U_{fs}}{U_m} \omega_m \tag{5}$$

The damping ratio ζ is independent of scale factor, however.

Both the static and dynamic wings consisted of two parts: the main wing panel and the trailing-edge tab. The tab consisted of three span segments numbered 1, 2, and 3, as shown in figure 1. Different combinations of tab segments could be used for the control surface to provide different amounts of control power $(\partial C_m/\partial\delta)_\alpha$.

The basic static stability of the wing, dC_m/dC_L, may be changed in several ways. Since dC_m/dC_L is equivalent to the static margin $\bar{x}_{ac} - \bar{x}_o$, these include changes in both the aerodynamic center and the dimensionless pivot location. First, the main wing panel is provided with two physical pivot locations which, with the nominal tab chord length of 0.0457 m, have dimensionless pivot locations of 0.22 c and 0.24 c behind the wing leading edge. Second, by using other trailing edge tab segments of greater chord lengths (0.0584 and 0.0711 m), the total wing chord can be increased, thereby decreasing the dimensionless pivot location ($\bar{x}_o = x_o/c$). Finally, each tab segment has a different trailing-edge angle ϕ_{TE} (defined in fig. 3) which results in a different aerodynamic center location for each wing-tab combination. Table 1 lists the various configurations used in the tests.

TABLE 1.– MODEL CONFIGURATIONS

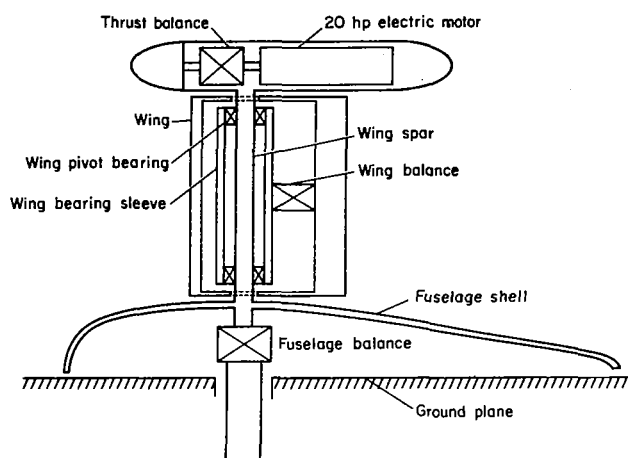| Static wing					
Basic pivot	Tab chord length, m	ϕ_{TE}, deg	Wing chord, m	$\bar{c}_t$	Dimensionless pivot location $\bar{x}_o$
0.24	0.0457	21.2	0.2286	0.20	0.24
.24	.0584	12.7	.2413	.242	.2274
.24	.0711	11.4	.2540	.280	.2160
.24	.0838	0	.2667	.314	.2057
.24[a]	.0838	0	.3949	.212	.2180
Dynamic wing					
0.22	0.0711	11.4	0.2540	0.280	0.198
.24	.0711	11.4	.2540	.280	.216

[a]Flap/slat extended.

5

Figure 4.- Schematic of model strain gage balance locations.

Three strain-gage balances contained in the model are illustrated schematically in figure 4. The primary six-component balance located within the fuselage supports the entire model. Propeller thrust force is measured by a single component balance contained in the nacelle. Isolated wing forces are measured with a six-component balance contained within the static wing; however, inertia limitations precluded its use in the dynamic wing. In order to determine isolated wing forces during the dynamic wing tests, the fuselage shell was disconnected from the primary balance and mounted directly on the ground plane. In this way, the primary balance recorded isolated wing forces, except for nacelle and propeller forces. For power-off tests this approach was satisfactory, since nacelle aerodynamic forces are minimal. For power-on tests, however, the large thrust forces rule out determination of aerodynamic forces on the dynamic wing.

Test Procedure

The tests were carried out in two parts. The first series employed the static wing to determine static stability and static floating response characteristics for a variety of configurations. The basic wing with the 0.24 c pivot was used with tab chord lengths of 0.0457, 0.0584, and 0.0711 m. Propeller tilt angles were varied between 0° and 60°. Higher angles were restricted due to slipstream recirculation effects within the tunnel test section. Tunnel velocity was 39.5 m/sec for most of the power-off tests. For the power-on tests, propeller RPM was varied in conjunction with tunnel velocity to achieve values of thrust coefficient (T_c'') that would represent typical flight conditions. The resulting velocities ranged from 6.25 to 19.76 m/sec. Lift, drag, and pitching moments were measured for the complete model and for the wing on respective balances.

The second series of tests used the dynamic wing to investigate the transient response and stall flutter of a free wing. Two basic wing-pivot positions, 0.22 c and 0.24 c were tested, each with the 0.0711 m tab chord length. Tab segments 1 and 2 were used to ensure high control power for inducing wing transients.

Dynamic characteristics were investigated as follows. Free oscillation frequency and damping ratio at low angles of attack in the linear aerodynamic regime were deduced from transient responses to step inputs. These were produced by displacing the wing from its trim angle of attack with an external probe and releasing it instantaneously. The motion was recorded with an oscillograph for subsequent measurement of the desired dynamic characteristics. This procedure was carried out for various trim angles of attack and tunnel velocities.

Stall flutter was investigated by attempting to induce oscillations for all tested configurations of the dynamic wing. Control tab deflections were used to initiate and control oscillation

6

amplitude, and to effect recovery. Power-on tests with the dynamically scaled wing were limited to static floating characteristics and investigation of the stall flutter phenomenon. No force measurements were obtained.

RESULTS AND DISCUSSION

Static Stability

The essential parameter for determining wing static stability is the aerodynamic center location, as shown by the results in appendix B.

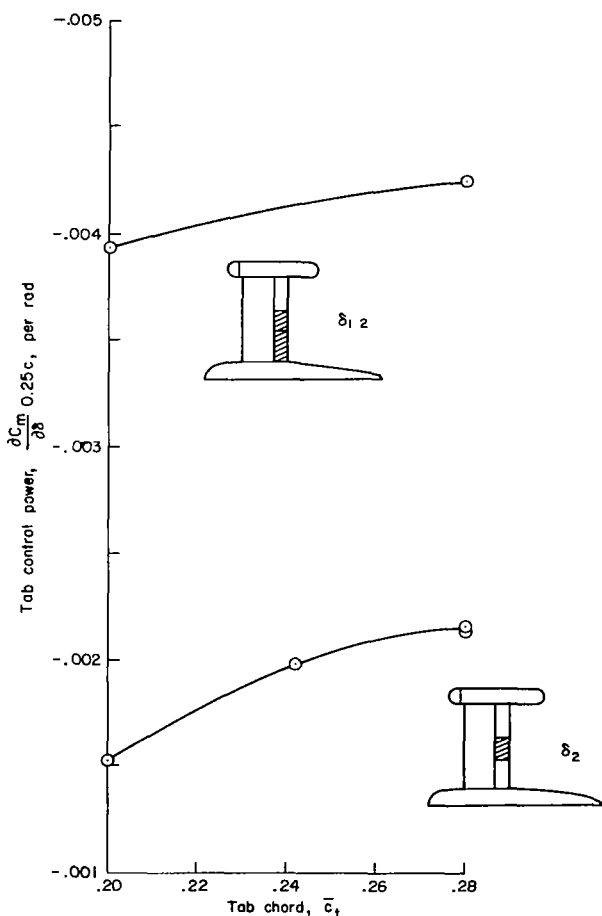$$\left(\frac{dC_m}{dC_L}\right)_\delta = -(\bar{x}_{ac} - \bar{x}_0) \tag{6}$$

Figure 5.- Wing tab control power variation with model configuration.

The static stability is defined as the slope of the C_m vs. C_L curve for constant tab deflection with the wing fixed. As equation (6) indicates, for a given pivot location, the static stability is dependent only on the aerodynamic center location. A variety of configurations of both the static and dynamic wings were tested in steady-state conditions and the static stability characteristics are presented as follows. For the static wing (in the fixed condition), the aerodynamic center is simply derived from the C_m vs. C_L curve, using equation (6).

For the dynamic wing, an indirect method of determining static stability is required since it was tested in the free-floating configuration. This method is based on wing static floating response characteristics and the equations derived in appendix B. The static stability is

$$\left(\frac{dC_m}{dC_L}\right)_\delta = -\frac{(\partial C_m/\partial\delta)_\alpha}{(\partial C_L/\partial\alpha)_\delta (d\alpha/d\delta)_{free}} \tag{7}$$

For this method the tab control power, $(\partial C_m/\partial\delta)_\alpha$, and lift curve slope, $(\partial C_L/\partial\alpha)_\delta$, are for the wing in the fixed condition. These parameters are obtained from the static wing data contained in appendix C. The tab control power, which is strongly dependent on the tab geometry, is shown in figure 5.

Table 2 presents the results for aerodynamic center location for the static and dynamic wings. Since airfoil geometry, in particular, the trailing edge angle ϕ_{TE}, is the major factor in determining

TABLE 2.– STATIC STABILITY ANALYSIS

Static wing								
c, m	U, m/sec	$\bar{x}_0$	$\bar{c}_t$	Spanwise tab segments	$\left(\dfrac{\partial C_L}{\partial\alpha}\right)_\delta$, rad⁻¹	$\left(\dfrac{\partial C_m}{\partial\alpha}\right)_\alpha$, rad⁻¹	dC_m/dC_L	$\bar{x}_{ac}$
0.2286	40	0.240	0.20	2		-0.10313	0	0.240
.2413	40	.2274	.242	2		-.13465	-.0194	.2468
.2540	10	.216	.28	2	4.58	-.14209	-.0390	.2550
.2540	40	.216	.28	2	4.83	-.14840	-.0367	.2527
.2286	20	.240	.20	1,2		-.23377[a]	.00564[a]	.234
.2540	20	.198	.28	1,2		-.29794[a]	-.0705[a]	.2685

Dynamic wing							
c,m	U, m/sec	$\bar{x}_0$	$\bar{c}_t$	Spanwise tab segments	$(d\alpha/d\delta)_{free}$	dC_m/dC_L	$\bar{x}_{ac}$
0.2540	28	0.198	0.28	1,2	-1.27	-0.0499	0.2479
.2540	28	.216	.28	1,2	-1.83	-.0325	.2484

[a]Based on data from reference 4.
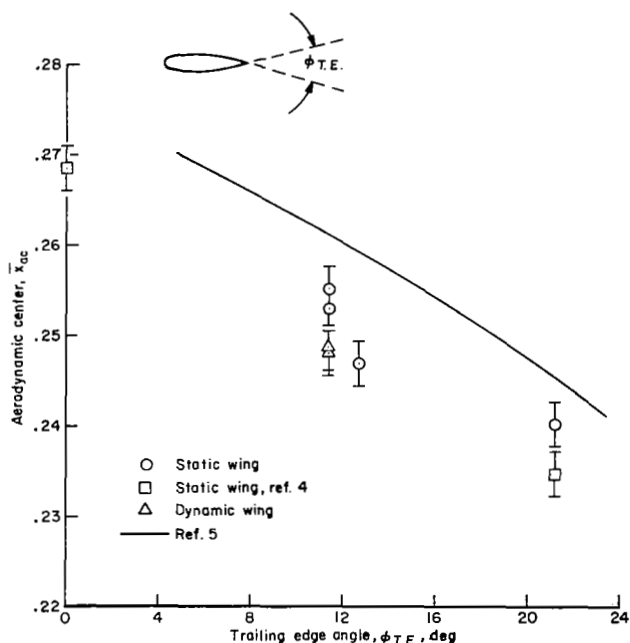
Figure 6.- Variation of aerodynamic center location with trailing-edge angle.

$\bar{x}_{ac}$, figure 6 is also presented to show the general trend of the results. Data from reference 5 for 17 percent thick airfoils are also included which substantiate the trend of the results. Variations in the experimental results can be attributed to several factors. Nonlinearities and experimental errors in the data reduce the accuracy of the slopes obtained by graphical means. Small variations were present in the airfoil contours and thickness ratio (17 to 19 percent), and finally, the Reynolds number was not constant for all of the data points. From the design point of view a rearward aerodynamic center is desirable, therefore these results indicate the benefit to be gained with a small trailing-edge angle.

The results shown on the linear characteristics of wing static stability are valid for low angles of attack and small tab deflections; but for large angles, especially those approaching stall, the effects of separation become significant. This is readily apparent in the pitching moment of the wing

δ₂, deg
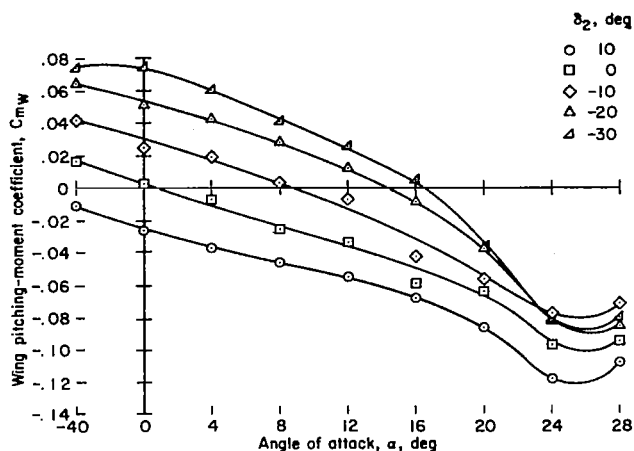- ○ 10
- □ 0
- ◇ -10
- △ -20
- ⊿ -30

Figure 7.- Wing pitching-moment coefficient versus wing angle of attack for several control tab deflections; static wing; pivot location 21.6 percent; $\delta_{13} = 0°$; propeller off; $U = 39.5$ m/sec.

as shown in figure 7. The independent variable is angle of attack, and the slope $dC_m/d\alpha$ is the angle-of-attack stability. In the linear region, it is equal to the wing static stability times the lift-curve slope. In the stall region, at high angles of attack, it is a more accurate parameter than dC_m/dC_L, since it is independent of the nonlinearity in the lift curve. This figure illustrates the large increase in magnitude of angle-of-attack stability for $16° < \alpha < 25°$. At higher angles, the slope becomes zero and then positive which means that the wing is statically unstable. These variations can be expected to have a significant effect on the wing dynamic characteristics.

Dynamic Characteristics

Transient responses— As explained in the section on test procedure, transient responses were induced by using an external probe to suddenly release the wing from an untrimmed angle of
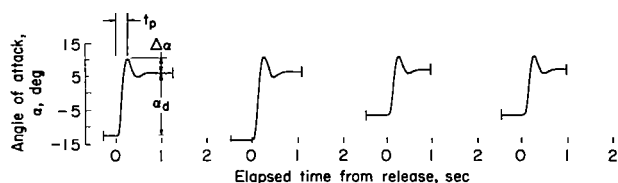
Figure 8.- Wing transient dynamic responses; propeller off; pivot location 19.8 percent; $U = 19.8$ m/sec; $\delta_{12} = -10°$.

attack. Typical time histories for the dynamic wing with the 0.198 c pivot (4.99 percent static margin) are illustrated in figure 8 for a trim angle of attack of approximately 6°. The four cases included indicate the degree of consistency between individual responses. Variations in the responses are caused by wind tunnel turbulence and small amounts of friction in the wing pivot bearings.[1]

The frequency and damping ratio of an equivalent second-order dynamic system were determined from measurements of the magnitude and time of the response overshoot, together with the following equations. The results obtained were averaged from several responses.

$$\left|\frac{\Delta\alpha}{\alpha_d}\right| = e^{-\pi\zeta/\sqrt{1-\zeta^2}} \tag{8}$$

$$\omega = \frac{\pi}{t_p} \tag{9}$$

---

[1] In some cases, friction could become excessive due to improper alinement of the wing. These instances were readily apparent in the data and were simply excluded from consideration.

Here, t_p is the time from release to the first transient overshoot peak; α_d is the deviation from the trim condition at the instant of release; and $\Delta\alpha$ is the magnitude of the overshoot. These parameters are illustrated in figure 8. Figure 9 summarizes the results together with theoretical predictions.
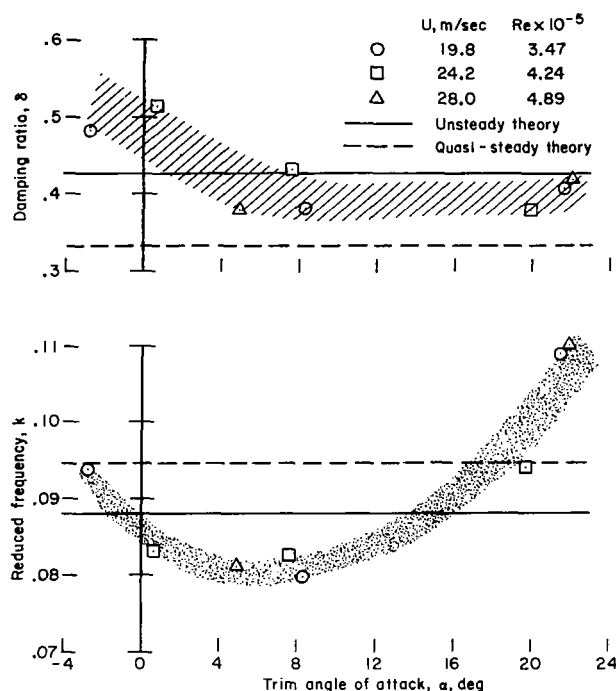

Figure 9.- Variation of measured transient response characteristics with trim angle of attack for several velocities and comparison with linear theory; dynamic wing; pivot location 19.8 percent; static margin 4.99 percent.

The experimental data illustrate the effect of trim angle of attack on the frequency and damping at several tunnel velocities. The variation of frequency with trim angle of attack results primarily from nonlinear aerodynamics. The pronounced increase in static stability at high angles of attack shown in figure 7 explains the corresponding increase in the free-wing pitching frequency. The variation of damping ratio is not as easily explained, however, since an increase in natural frequency should result in a reduction in damping ratio if the total damping is constant.

In the linear aerodynamic region at moderate trim angles of attack, the experimental results can be compared with quasi-steady and unsteady aerodynamic theory. The experimentally derived values for wing static stability given in table 2 are used as the basis for the theoretical calculations outlined in appendix A.

Even for moderately low reduced frequencies ($k \sim 0.1$), unsteady aerodynamic theory differs appreciably from quasi-steady theory. The damping ratio in figure 9 is in reasonably good agreement with more exact unsteady theory, although the quasi-steady theory is deficient by about 15 percent. For moderate trim angle of attack ($0° < \alpha < 12°$), the damped natural frequency is overpredicted by both quasi-steady and unsteady theory; however, the latter is more accurate. This is in agreement with reference 1, which considered the effects of unsteady aerodynamics on dynamic characteristics of free wings. These findings are important to the design of free-wing aircraft, for unless unsteady aerodynamics are considered, predictions of wing pitching frequency and gust alleviation effectiveness can be overoptimistic.

Discrepancies in the correlation between the experimental results and the unsteady theory may be traced to several factors. Experimental errors occur from the effects of wing-pivot friction and from measurements of oscillograph data records. In addition, unsteady aerodynamic theory is strictly correct only for simple harmonic motion, and some discrepancies are inherent in applying it to transient motion. Finally, the method used to account for the three-dimensional character of the low aspect-ratio model is only approximate, and to a degree the theoretical predictions are subject to this factor.

10

Stall flutter— A major objective of the investigation was to observe the dynamic characteristics of the free wing under stalled trim conditions. Nearly all configurations with adequate static stability and dynamic response at moderate angles of attack readily exhibited limit-cycle oscillations when trimmed at high angles of attack. The term *stall flutter* is used to describe self-sustained oscillations in the stall region associated with unsteady flow separation.

The limit-cycle oscillations were initiated with control tab inputs; generally, a large trim angle of attack was sufficient to precipitate the motion. In some cases, transient overshoots from large control inputs were required, and, in a few instances stall flutter could not be initiated. Flutter was easily terminated by reducing the control tab deflection. Large oscillation amplitudes of 15° to 20° were typical; periodic separation and reattachment occurred over the entire upper wing surface. (This fact was confirmed by the study of wool tufts attached to the wing surface.)

Various features of the stall flutter limit cycle are shown by time histories of representative oscillation records. For these data, the tab chord is 0.0711 m, $x_0 = 0.198$, and the control tab comprises span segments 1 and 2.

The first example in figure 10(a) is a power-off condition with the nacelle removed. The first response is not of sufficient magnitude to produce stall flutter but the wing is partially stalled at its trim angle of attack. The random separated flow did produce an irregular pitching response of the wing until the control tab deflection was reduced. The next input resulted in a larger initial response of the wing, and stall flutter did occur. The oscillation quickly reached a nearly constant amplitude until it was terminated with a reduction in tab deflection. Finally, a third and smaller input produced a *positively* damped transient response because of the low trim angle of attack.

The second time history (fig. 10(b)) illustrates a series of stall flutter sequences initiated and terminated with control tab inputs for a power-on condition with zero free-stream velocity. This case indicates that the propeller slipstream itself can sustain stall flutter.
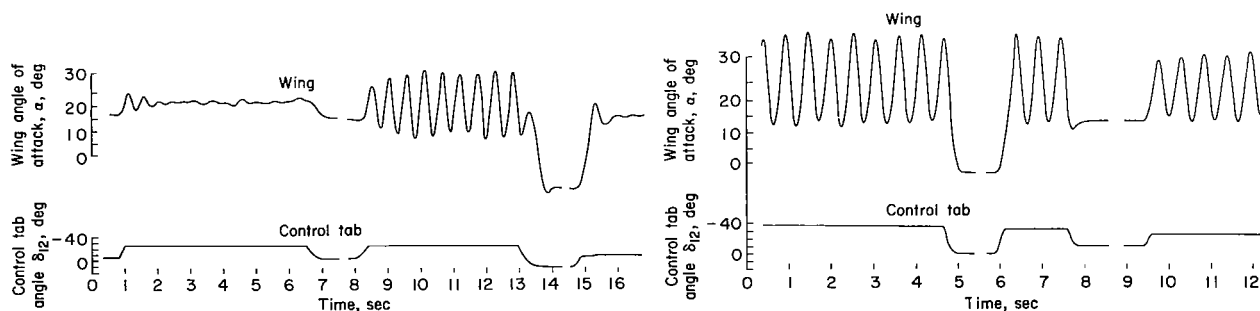
(a) Propeller and nacelle off; U = 19.8 m/sec.   (b) Power on; U = 0; q_s = 74.7 N/m^2.

Figure 10.- Stall flutter time histories; dynamic wing; pivot location 19.8 percent, $\alpha_p = 0°$.

The third sequence, a power-on condition (fig. 10(c)), illustrates the occasionally inconsistent behavior of the stall flutter phenomenon. In the first portion stall flutter is initiated, but then becomes damped, while a subsequent oscillation with the same control-tab deflection continues. It is possible that the small control reduction during the first response was responsible for flutter decay. These responses do indicate different types of behavior for a given control-tab angle.

The final time history (fig. 10(d)) is for a power-on condition that would not sustain stall flutter but is included in the interest of completeness. The nonlinear behavior is evident in the very low initial damping of the transient responses. No explanation is given for the absence of stall flutter except that possibly the initial response amplitude was too small. For most of the configurations tested, there was no difficulty in initiating stall flutter.

For the few instances when pivot bearing friction was excessive, erroneous data was readily apparent. However, small amounts of friction could not be identified and may account for some irregularities in the data, particularly when stall flutter was marginal (figs. 10(c) and (d)).

(c) Power on; U = 13.1 m/sec; $T_c'' = 0.34$.

(d) Power on; U = 8.84 m/sec; $T_c'' \cong 0.1$.
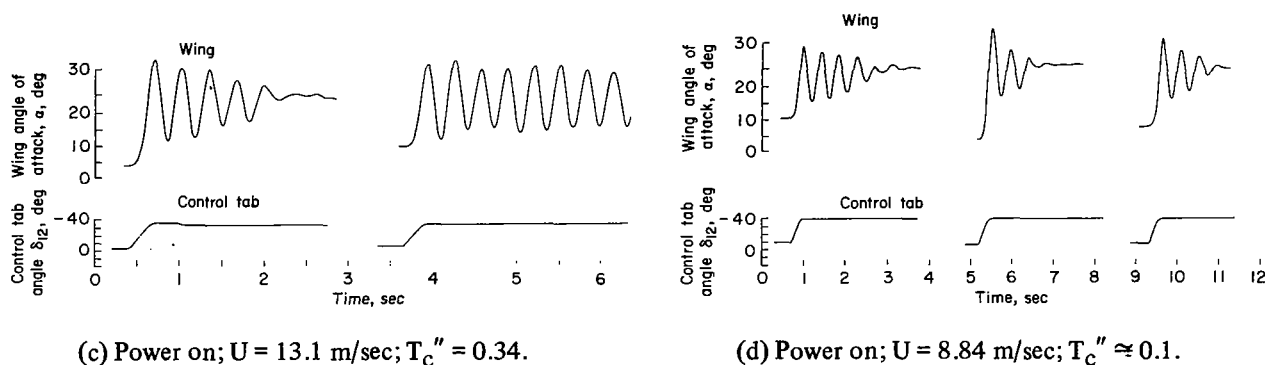
Figure 10.- Concluded.

Figures 11(a) and 11(b) summarize the stall flutter results of both configurations (x_o = 0.198 and 0.216) for the power-off condition at several velocities. Superimposed on the static floating-response curves are the approximate peak-to-peak excursions of the stall flutter limit cycles. These plots confirm several characteristics of the limit cycle identified from the time histories. First, for moderate control-tab deflections and moderate trim angles of attack, the wing shows no tendency to flutter. It is significant that the upper limit of this range of trim angles of attack (i.e., the flutter threshold) includes the lower part of the stall region. The well damped behavior of the wing in this region ensures that transient responses and external excitation (such as atmospheric turbulence) will not produce flutter. Furthermore, it may be desirable to limit control tab deflection on free-wing aircraft to preclude stall flutter by restricting the maximum trim angle of attack. Since this angle of attack is already near the maximum trimmed lift coefficient, there would be little penalty in lift performance.

A second result obtains for larger control tab deflections and corresponding trim angles of attack. In this region the wing is essentially stalled, but stable trimmed conditions are possible. Small amplitude transients are damped, but larger amplitude oscillations produced by control inputs or turbulence rapidly develop into stall flutter oscillations. A comparison of the damping ratio results of figure 9 with figure 11(b), clearly shows that low amplitude transients are well damped, while for the same trim angle of attack a large amplitude transient will produce stall flutter. This type of behavior was not observed, however, for negative trim angles of attack.

12

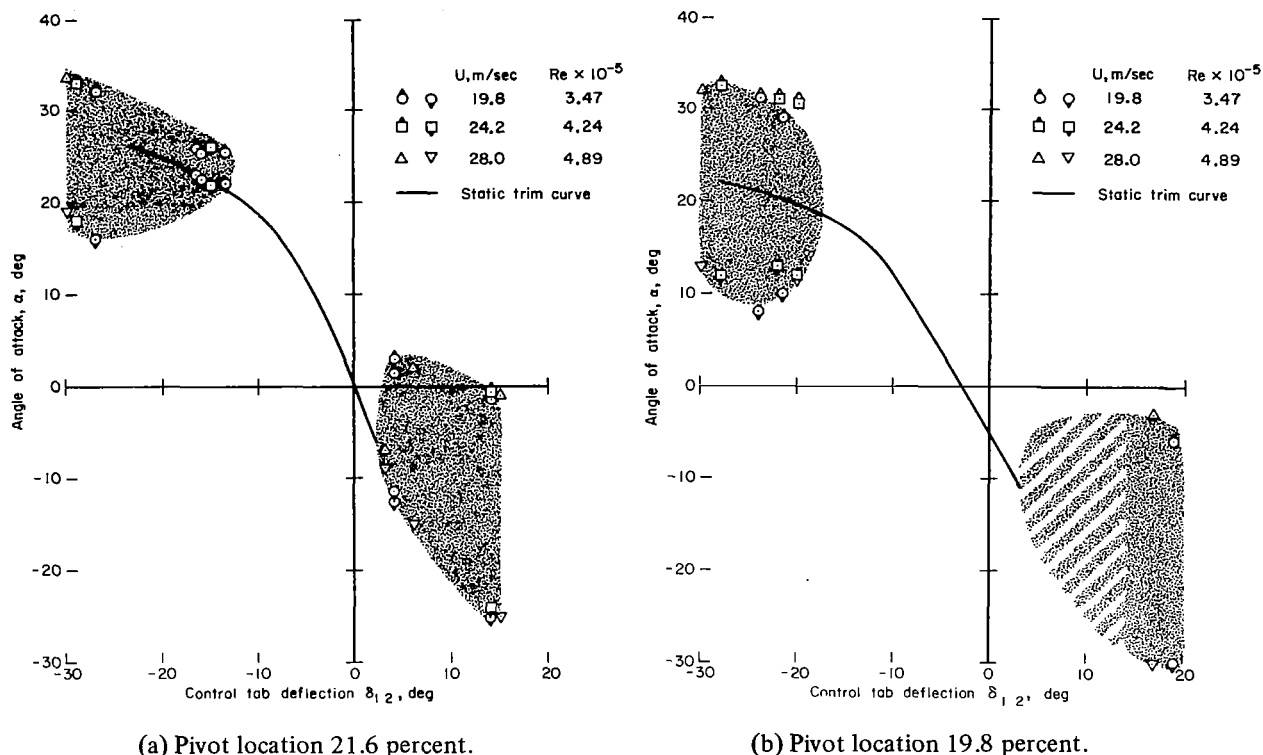(a) Pivot location 21.6 percent.　　　　(b) Pivot location 19.8 percent.

Figure 11.- Stall flutter oscillation envelopes at several velocities; dynamic wing; power off; nacelle removed.

A third type of stall flutter behavior was produced for the greatest control tab deflections. Stable trimmed conditions were not possible, and transients were not required to initiate the stall flutter oscillation. Termination of stall flutter was immediate, however, upon reduction of the control tab deflection below the flutter threshold.

Wing static stability (dC_m/dC_L = -0.0325 and -0.0499) does not have a large influence on stall flutter; however, the less stable configuration (x_0 = 0.216) does exhibit smaller amplitude oscillations and also a minor form of stall flutter of less than 5° peak-to-peak amplitude for trim angles just above the flutter threshold (fig. 11(a)).

The above observations lead to certain insights about the stall-flutter oscillation. Since the oscillation includes the stall region, it is reasonable that negative pitch damping[2] produced by unsteady flow separation and reattachment is responsible for limit cycle oscillations. In fact, measurements of pitch damping given in reference 3 for airfoils forced to oscillate in simple harmonic motion substantiate this conclusion. Although the test conditions, airfoil geometry, and oscillation waveforms are not identical, the two cases are sufficiently similar to support this hypothesis. The degree of similarity of relevant parameters is illustrated by the following table:

---

[2] This should not be confused with the damping ratio of figure 9 discussed previously. Here, negative pitch damping refers to the net aerodynamic energy transferred to the airfoil per oscillation cycle and is proportional to $\oint C_m\, d\alpha$, as discussed in reference 3.

13

Parameter	Reference 3	Present test
Oscillation amplitude	$9.6°$	$20°$
Mean or trim angle of attack	$19.78°$	$20°$
Reduced frequency	0.115	0.15
Mach number	0.2	0.06
Airfoil section	23010-1.58	$63_2A_{(015)}$-219 mod.
Airfoil thickness ratio	0.102	0.171

For the example from reference 3, the cycle pitch damping is negative, indicating that a limit cycle would exist for a free-floating airfoil oscillating with sufficient amplitude at the proper frequency (governed by the static stability and inertia). The negative damping at the *forced* amplitude of 9.6° implies that the oscillation amplitude for a free-floating airfoil would increase until the net cycle damping was reduced to zero, and a stable limit cycle resulted. This explains the large amplitude of the present stall flutter oscillation.

Some mention at least should be given to the effects of Reynolds number and wing inertia. The tests were conducted at low velocities; at 20 m/sec, the Reynolds number is 3.5×10^5. At higher Reynolds numbers the flow separation and pitch damping characteristics could be altered. However, negative pitch damping is also shown in reference 3 for relatively low Reynolds numbers of 2.6×10^6 at $M = 0.2$, and, in general, the pitch damping is not highly dependent on Reynolds number variations.

Inertial characteristics of the model were obtained from dynamic scaling of a representative full scale V/STOL concept with a wing relative mass parameter $\bar{I}$ of 21.6. The effect of higher or lower mass would alter the wing natural frequency, analogous to changes in pivot location. Again, reference 3 indicates that moderate changes in frequency would not substantially change the pitch damping characteristics.

Another factor influencing the stall flutter phenomenon may be the static angle-of-attack stability characteristics presented in figure 7. Neutral and then negative stability at high angles of attack can result in nonlinear limit cycle oscillations even for a system with positive linear damping. More likely, however, the region of neutral stability allows large transients to occur which, in turn, precipitate the stall flutter oscillation. Furthermore, comparison of figures 7 and 11(a) reveals that the region of high trim angle of attack where only limit cycle behavior is present corresponds to the angle-of-attack range for negative angle-of-attack stability. Therefore, reduced static stability at high angles of attack probably facilitates the onset of stall flutter oscillations.

High Lift Devices

Figure 12 presents the results of a brief optimization study of high-lift device performance for the static wing. The airfoil geometry is illustrated in figure 3. Although the leading-edge slat is conventional, static trim of the free wing prohibits large trailing-edge flap deflections which cause large negative pitching moments. Therefore, the trailing-edge flap was moved rearward without deflection 0.097 m, thereby increasing the wing area 36.4 percent. A slot was provided to inhibit trailing-edge separation, and the tab chord was increased to 0.0838 m to increase the control power for trim at maximum lift. The pivot location, 0.218 c is measured from the leading edge of the
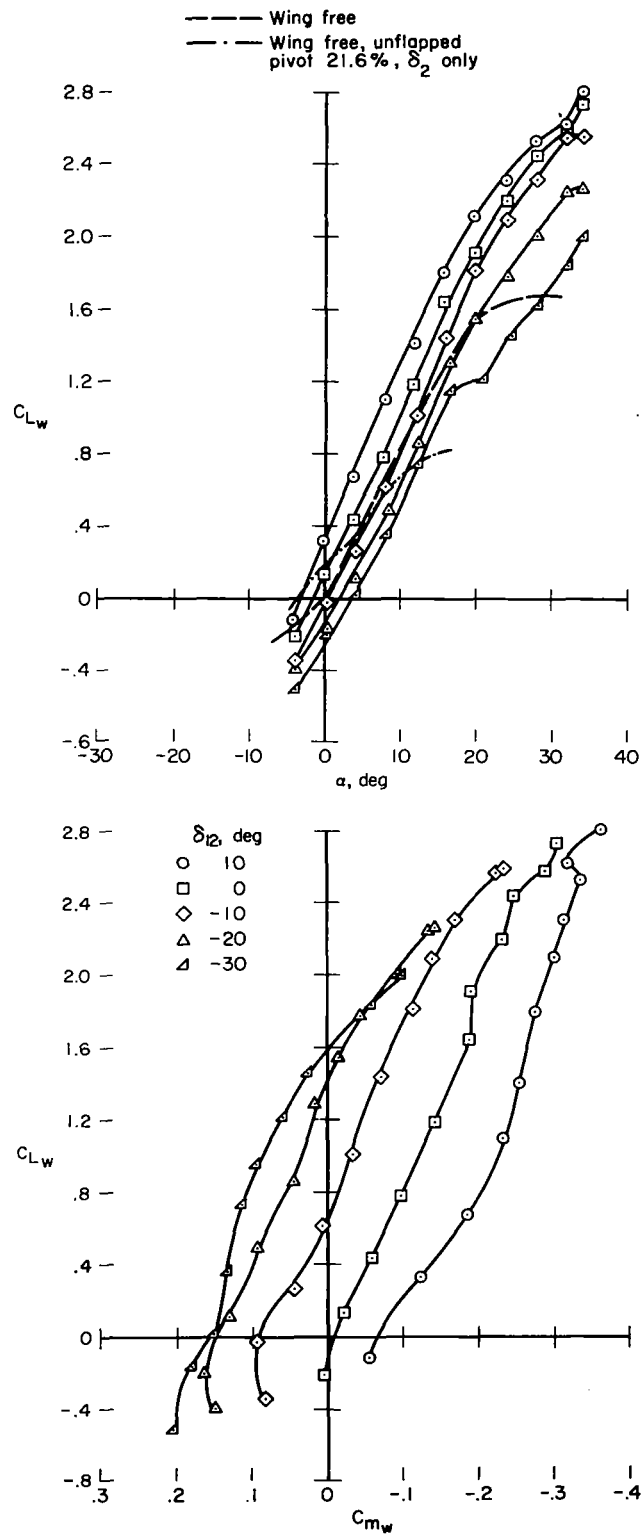
Figure 12.- Wing lift and pitching-moment coefficient with flap and slat extended; static wing; pivot location 21.8 percent; δ_3 = -12.5°; propeller off; U = 39.5 m/sec.

extended slat and made dimensionless by the total wing chord. (The lift coefficient is based on the unflapped wing reference area.) With the wing in the free-floating condition, the maximum lift coefficient is increased approximately 101 percent over that of the unflapped configuration. The effectiveness of the leading-edge slat is indicated by the fact that this percentage is greater than would be expected on the basis of the increased wing area alone. The large reduction, however, in $C_{L_{max}}$ of the flapped configuration, from fixed to the free-floating condition, clearly indicates the adverse lift penalty of the control tab used for trimming the free-floating wing.

The effects of high-lift devices on stall flutter were not evaluated with the dynamically scaled wing, although instances of stall flutter were observed with the static wing.

Power Effects

A potential advantage of the floating wing for tilt-propeller or tilt-wing V/STOL concepts is a reduction of wing download or separated flow in transition flight regimes. This results from the wing rotating freely in pitch to maintain a reasonable angle of attack, irrespective of the magnitude and direction of the propeller slipstream relative to the free-stream velocity.

The wind-tunnel tests indicate that this behavior is realized in most cases; the floating capability of the wing does act to eliminate the undesirable effects of propeller-wing interference on the wing lift characteristics. The results also show, however, that the effects of propeller tilt angle and thrust coefficient on the wing float angle and static response characteristics are not obvious. The wing float angle should increase with an increase in either thrust coefficient or propeller tilt angle. Furthermore, the wing should aline itself in a direction intermediate between the free-stream velocity and the propeller tilt angle, at least for small control tab deflections.

Figures 13(a) and (b) (derived from wind-tunnel test data in appendix C) depict floating angle versus propeller tilt angle at various control tab settings and thrust coefficients, for pivot locations of 0.216 c and 0.2274 c, respectively. The effects of thrust coefficient have no consistent trends. Propeller tilt angle effects are also unusual in most cases, generally contradicting the reasoning outlined above, in that the wing alinement diverges strikingly from the propeller direction at high tilt angles. There are two possible reasons for this behavior. First, the propeller rotation direction is such that the slipstream swirl tends to reduce the wing floating angle; however, this reduction cannot account for the unusual gradients of wing angle of attack with respect to propeller tilt angle.

The other reason is that the airfoil pressure distribution on the lower surface near the leading edge may experience an abnormal suction peak due to local impingement of the slipstream from above. The resulting negative pitching moment might then offset the normal positive moment due to the reduced effective angle of attack caused by the slipstream velocity vector.

The effects of propeller slipstream on static stability can be indirectly ascertained from α vs. δ trim curves. The gradient $(d\alpha/d\delta)^{-1}$ is directly proportional to static stability. For low propeller tilt angles, the effect of power on the trim gradient is small; however, at the high tilt angle of 60°,
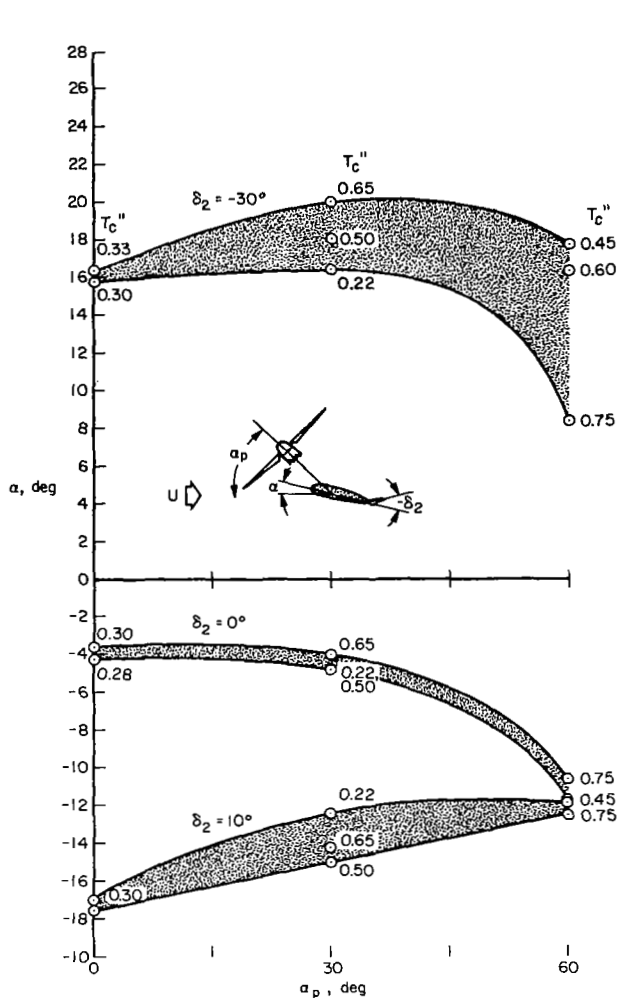
(a) Pivot location 21.6 percent.
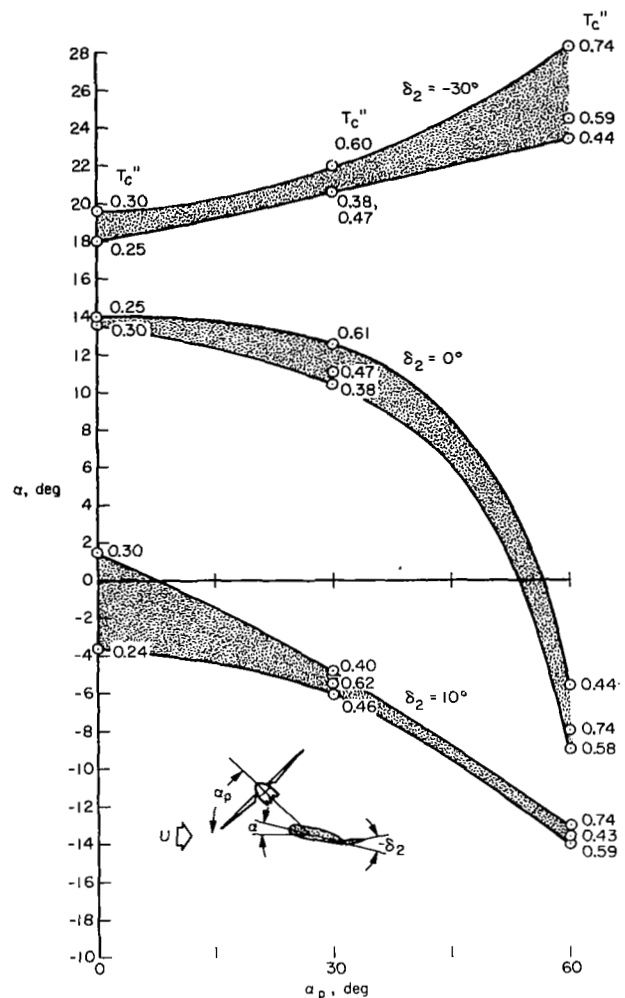
(b) Pivot location 22.74 percent.

Figure 13.- Effect of thrust coefficient and propeller tilt angle on free wing float angle for several control tab deflections; static wing; $\delta_{13} = 0°$.

stability is substantially reduced. In addition, the slipstream produces a highly nonlinear wing floating response curve. Figures 14(a) and (b) illustrate the effect of propeller tilt angle on the gradient of the floating response for pivot locations of 0.216 c and 0.2274 c, respectively.

SUMMARY OF RESULTS

At large trim angles of attack and for a variety of test conditions and configurations, the free-floating dynamic wing exhibited large amplitude (15° to 20°) limit cycle oscillations. Analyses

17

(a) Pivot location 21.6 percent.

(b) Pivot location 22.74 percent.
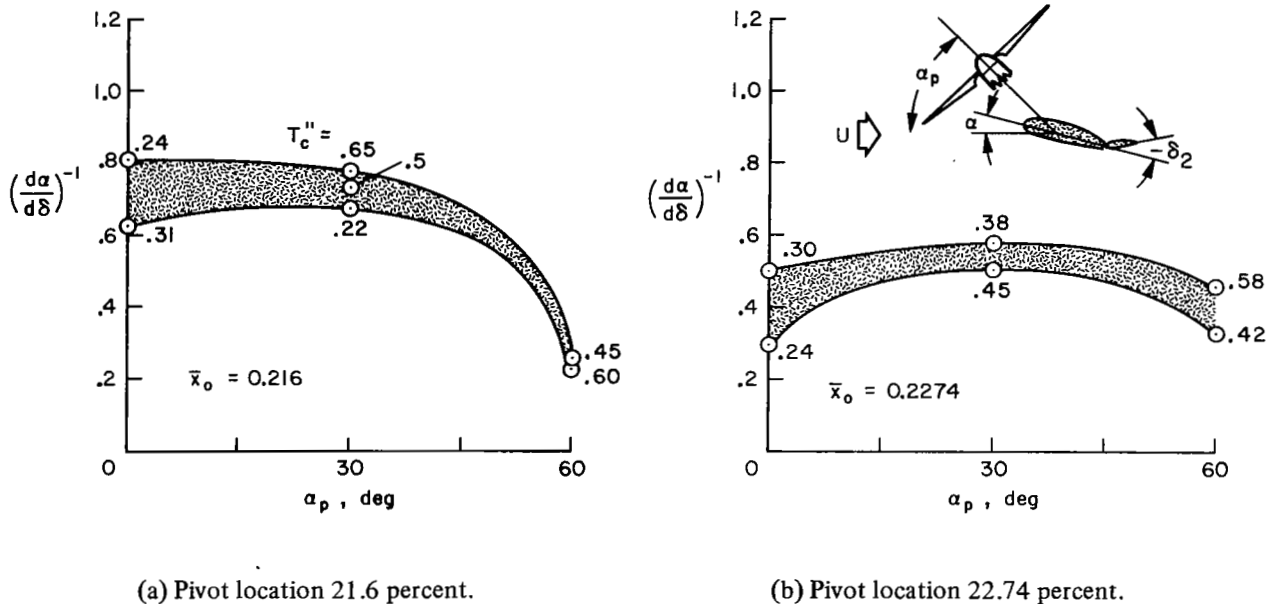
Figure 14.- Effect of thrust coefficient and propeller tilt angle on free-wing stability; static wing; $\delta_{13} = 0°$.

indicate that negative pitch damping from periodic flow separation, aggravated by loss of static stability at the high trim angles of attack, is responsible for stall flutter. Reducing the control tab deflection is an effective way of terminating the oscillations by reducing the trim angle of attack of the wing.

Transient responses at low trim angles of attack were moderately damped ($\zeta \simeq 0.4$) for static margins of 0.035 and 0.05. Comparison of frequency and damping with theoretical calculations confirms that unsteady aerodynamic theory affords better correlation than quasi-steady aerodynamic theory.

For power-on conditions, free-floating capability is effective in preventing flow separation and buffeting at high propeller tilt angles. However, the effects of propeller slipstream on the wing floating angle indicate that there are complex propeller-wing aerodynamic interactions.

Certain practical considerations indicated by the results are important for implementing the free-floating wing concept. Stall flutter cannot be tolerated and, as shown, might be prevented by suitable control tab limiting to prevent trim angles of attack greater than the flutter threshold. Other possible solutions are modified airfoils or mechanical dampers at the wing pivot. Control deflection limits would not seriously reduce the wing-lift capability since the flutter threshold is very near $C_{L_{max}}$.

The requirement for trim of the free wing does reduce the lifting capability substantially, but high-lift devices are quite effective.

Finally, the beneficial effect of reduced trailing-edge angle on aerodynamic center location is confirmed. As discussed earlier, this fact could be used to reduce static balance requirements and help reduce wing inertia.

Ames Research Center
   National Aeronautics and Space Administration
         and
U. S. Army Air Mobility R & D Laboratory
   Moffett Field, Calif., 94035, January 24, 1972

APPENDIX A

QUASI–STEADY AND UNSTEADY AERODYNAMIC THEORY

A brief description of two methods used to calculate the frequency and damping ratios for wing transient motion follows. The governing differential equation of motion for a freely pivoted wing acted upon only by aerodynamic moments is

$$-I\ddot{\alpha} + M_{aero} = 0 \qquad (A1)$$

For a two-dimensional, thin airfoil undergoing simple harmonic motion in pitch only, the unsteady aerodynamic moment per unit span according to Theodorsen's theory (ref. 6) is

$$M_{aero} = \pi\rho b^2\left[-Ub\left(\frac{1}{2} - a\right)\dot{\alpha} - b^2\left(\frac{1}{8} + a^2\right)\ddot{\alpha}\right]$$

$$+ 2\pi\rho Ub^2\left(a + \frac{1}{2}\right)C(k)\left[U\alpha + b\left(\frac{1}{2} - a\right)\dot{\alpha}\right] \qquad (A2)$$

The pitching axis is located a distance equal to ab behind the airfoil midchord; hence, $a = 2\bar{x}_0 - 1$. Since thin airfoil theory implies that the aerodynamic center is located at the quarter chord, equation (A2) can be generalized for an arbitrary aerodynamic center location using the following equation

$$a = -2(\bar{x}_{ac} - \bar{x}_0) - \frac{1}{2} \qquad (A3)$$

The three-dimensional effect of the finite wing on equation (A2) is approximated by a reduction factor (e = 0.71) equivalent to the ratio of the wing lift-curve slope to the two-dimensional value (2π). Equations (A1) through (A3) yield the following complex differential equation for the wing pitching motion.

$$\left(\frac{I}{e} + C\right)\ddot{\alpha} - B\left[1 - 2\left(a + \frac{1}{2}\right)(F + iG)\right]\dot{\alpha} - A(F + iG)\alpha = 0 \qquad (A4)$$

where

$$A = -2\pi\rho U^2 b^2\left(a + \frac{1}{2}\right) \qquad (A5)$$

$$B = \pi\rho Ub^3\left(a - \frac{1}{2}\right) \qquad (A6)$$

20

$$C = \pi \rho b^4 \left(\frac{1}{8} + a^2 \right) \tag{A7}$$

A solution of the form $\alpha = \alpha_0 e^{\lambda t}$, where $\lambda = \eta + i\omega$, is assumed and substituted into equation (A4). The resulting real and imaginary parts of the equation are individually equated to zero and give two equations for the frequency and damping, ω and η.

$$\eta = \frac{B\omega\{1 - 2[a + (1/2)]F\} + AG}{2\omega[(I/e) + C] - 2[a + (1/2)]BG} \tag{A8}$$

$$\omega^2 - \frac{2[a + (1/2)]BG}{(I/e) + C} + \frac{B\eta\{1 - 2[a + (1/2)]F\} + AF}{(I/e) + C} - \eta^2 = 0 \tag{A9}$$

Since $F(k)$ and $G(k)$ are functions of ω, these equations are solved iteratively, beginning with the approximation $k = 0$, and $F = 1.0$, $G = 0$. This approximation is usually referred to as the quasi-steady case. Equation (A4) then becomes real instead of complex and can be written in the following standard form

$$\ddot{\alpha} + 2\zeta\omega_n\dot{\alpha} + \omega_n^2\alpha = 0 \tag{A10}$$

The undamped natural frequency ω_n and damping ratio ζ are then obtained directly. The standard conversion from the damping and damped natural frequency is

$$\zeta = \frac{\eta}{\sqrt{\omega^2 + \eta^2}} \tag{A11}$$

$$\omega_n = \omega \sqrt{1 - \zeta^2} \tag{A12}$$

The solution of equation (A4) for transient motion is only approximate since the aerodynamic moment is for purely harmonic oscillations. In this condition, the wake consists of an infinite sheet of periodic vorticity extending behind the airfoil. When an airfoil is suddenly released from an out-of-trim condition, the unsteady wake is of finite length, and the strength of vorticity varies with time as well as distance behind the airfoil. However, these calculations are considered adequate for illustrating the major differences between unsteady and quasi-steady theory when compared to the experimental data.

APPENDIX B

STATIC STABILITY PARAMETERS

The equations used to calculate the static stability and control characteristics given in table 2 will be derived. Of primary interest are expressions that relate the wing static stability to the various lift and moment derivatives of the wing and control tab. The aerodynamic center of the airfoil is also determined from measurements made for the wing in both the fixed and free-floating condition.

The wing moment coefficient about x_{ac} can be written in terms of the moment about the pivot location as follows:

$$C_{m_{ac}} = C_m + C_L \frac{x_{ac} - x_o}{c} \tag{B1}$$

Differentiating with respect to C_L and noting that $dC_{m_{ac}}/dC_L = 0$, by definition, we have

$$\frac{dC_m}{dC_L} = -(\overline{x}_{ac} - \overline{x}_o) \tag{B2}$$

This equation shows the direct relationship between wing static stability and aerodynamic center. The quantity $(\overline{x}_{ac} - \overline{x}_o)$ is sometimes referred to as the wing static margin and is simply the dimensionless distance between the aerodynamic center and the pivot.

For a fixed wing, the static stability is easily determined from the slope of the C_m vs. C_L curve in the linear region, but for a free-floating wing, the pitching moments must vanish, and this technique cannot be used. An alternative formulation for the static stability may be developed as follows. The lift and moment coefficients are functionally dependent on angle of attack and control tab deflection, thus

$$C_L = C_L(\alpha, \delta) \tag{B3}$$

$$C_m = C_m(\alpha, \delta) \tag{B4}$$

Taking total differentials,

$$dC_L = \left(\frac{\partial C_L}{\partial \alpha}\right)_\delta d\alpha + \left(\frac{\partial C_L}{\partial \delta}\right)_\alpha d\delta \tag{B5}$$

$$dC_m = \left(\frac{\partial C_m}{\partial \alpha}\right)_\delta d\alpha + \left(\frac{\partial C_m}{\partial \delta}\right)_\alpha d\delta \tag{B6}$$

The partial derivatives are sometimes called stability derivatives and are the lift curve slope, control tab adverse lift, angle-of-attack stability, and tab control power, respectively.

In the free-floating condition, the moment vanishes ($dC_m = 0$), and equation (B6) yields the static floating response of the wing.

$$\left(\frac{d\alpha}{d\delta}\right)_{free} = -\frac{(\partial C_m/\partial \delta)_\alpha}{(\partial C_m/\partial \alpha)_\delta} \tag{B7}$$

The static stability requires the condition of constant tab deflection ($d\delta = 0$); hence equations (B5) and (B6) yield

$$\left(\frac{dC_m}{dC_L}\right)_\delta = \frac{(\partial C_m/\partial \alpha)_\delta}{(\partial C_L/\partial \alpha)_\delta} \tag{B8}$$

Combining equations (B7) and (B8) finally yields the static stability in terms of the free-wing floating response

$$\left(\frac{dC_m}{dC_L}\right)_\delta = -\frac{(\partial C_m/\partial \delta)_\alpha}{(\partial C_L/\partial \alpha)_\delta (d\alpha/d\delta)_{free}} \tag{B9}$$

The control power, $(\partial C_m/\partial \delta)_\alpha$, and lift curve slope, $(\partial C_L/\partial \alpha)_\delta$, must still be measured for the wing in the fixed condition.

APPENDIX C

STATIC TEST DATA

This appendix contains the static wind tunnel test data on which a portion of the figures and tables presented in the main text are based. Table 3 summarizes the data presented and is listed according to figure number.

TABLE 3.– STATIC TEST CONDITIONS AND CONFIGURATIONS

Figure	Wing pitch freedom	Wing type	Propeller tilt angle, α_p, deg	c_t, m	$\bar{x}_0$	ϕ_{TE}	Spanwise tab segments
15(a)	Fixed	Static	Prop off	0.0457	0.24	21.2	2
(b)	↓	↓	↓	.0584	.2274	12.7	2
(c)				.0711	.216	11.4	2
(d)	↓	↓		.0711	.216	11.4	2
16(a)	Free	Dynamic		.0711	.198	11.4	1,2
(b)		↓	↓	.0711	.216	11.4	1,2
17(a)			Nacelle off[a]	.0711	.198	11.4	1,2
(b)		↓	↓	.0711	.216	11.4	1,2
18(a)		Static	0	.0711	.216	11.4	2
(b)		↓	30	.0711	.216	11.4	2
(c)			60	.0711	.216	11.4	2
19(a)			0	.0584	.2274	12.7	2
(b)			30	.0584	.2274	12.7	2
(c)		↓	60	.0584	.2274	12.7	2
20	↓	Dynamic	0 and 45	.0711	.198	11.4	1,2

[a]Wing tip fairing added.
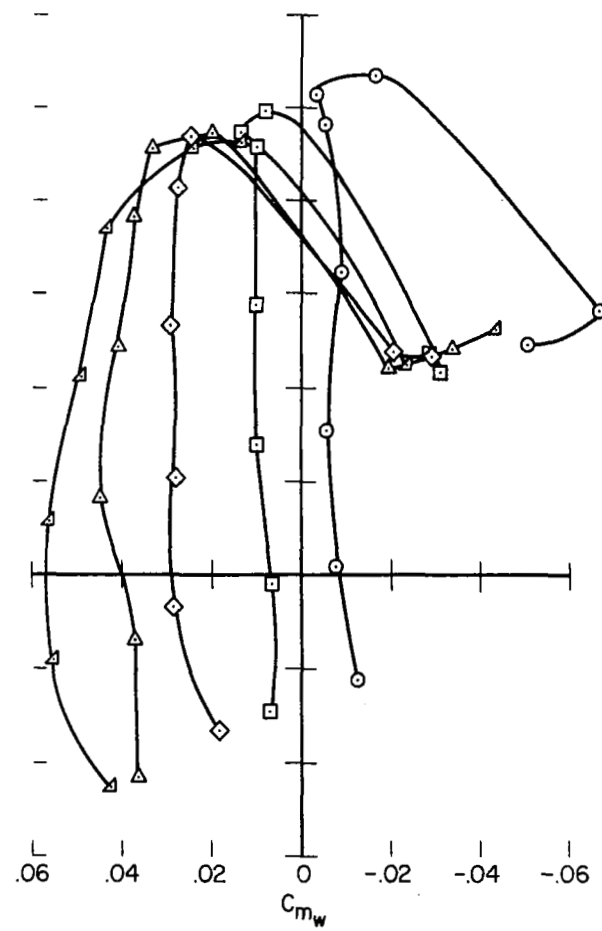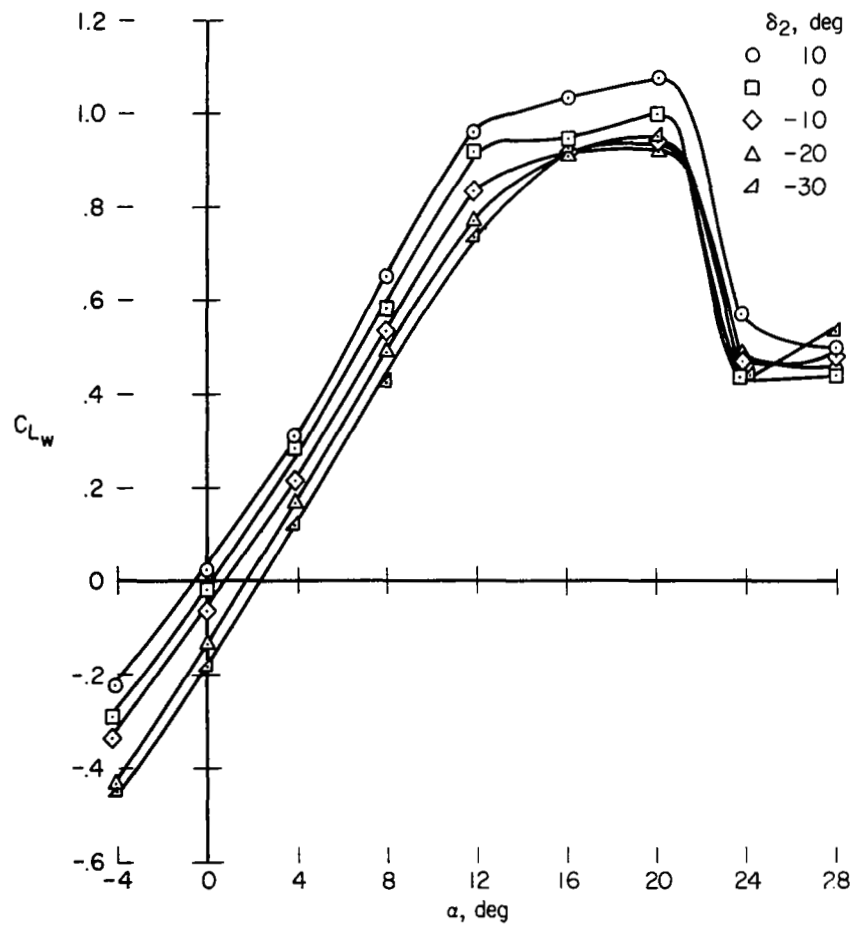
(a) Pivot location 24.0 percent; Re = 7.38×10^5.

Figure 15.- Lift and pitching-moment coefficient; static wing; propeller off; $\delta_{13} = 0°$.
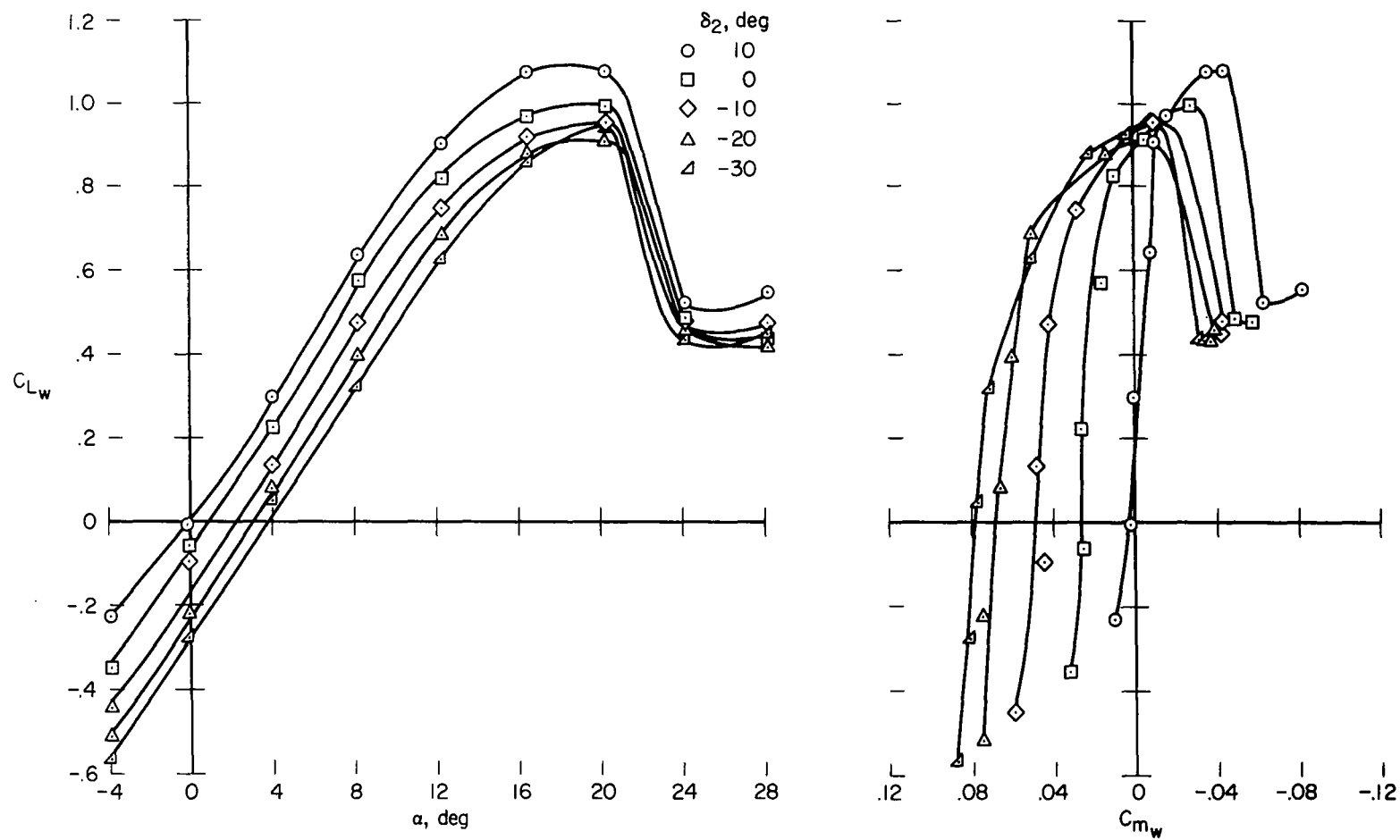
(b) Pivot location 22.74 percent; Re = 7.79×10^5.

Figure 15.- Continued.

δ_2, deg
- ○ 10
- □ 0
- ◇ -10
- △ -20
- ⊿ -30
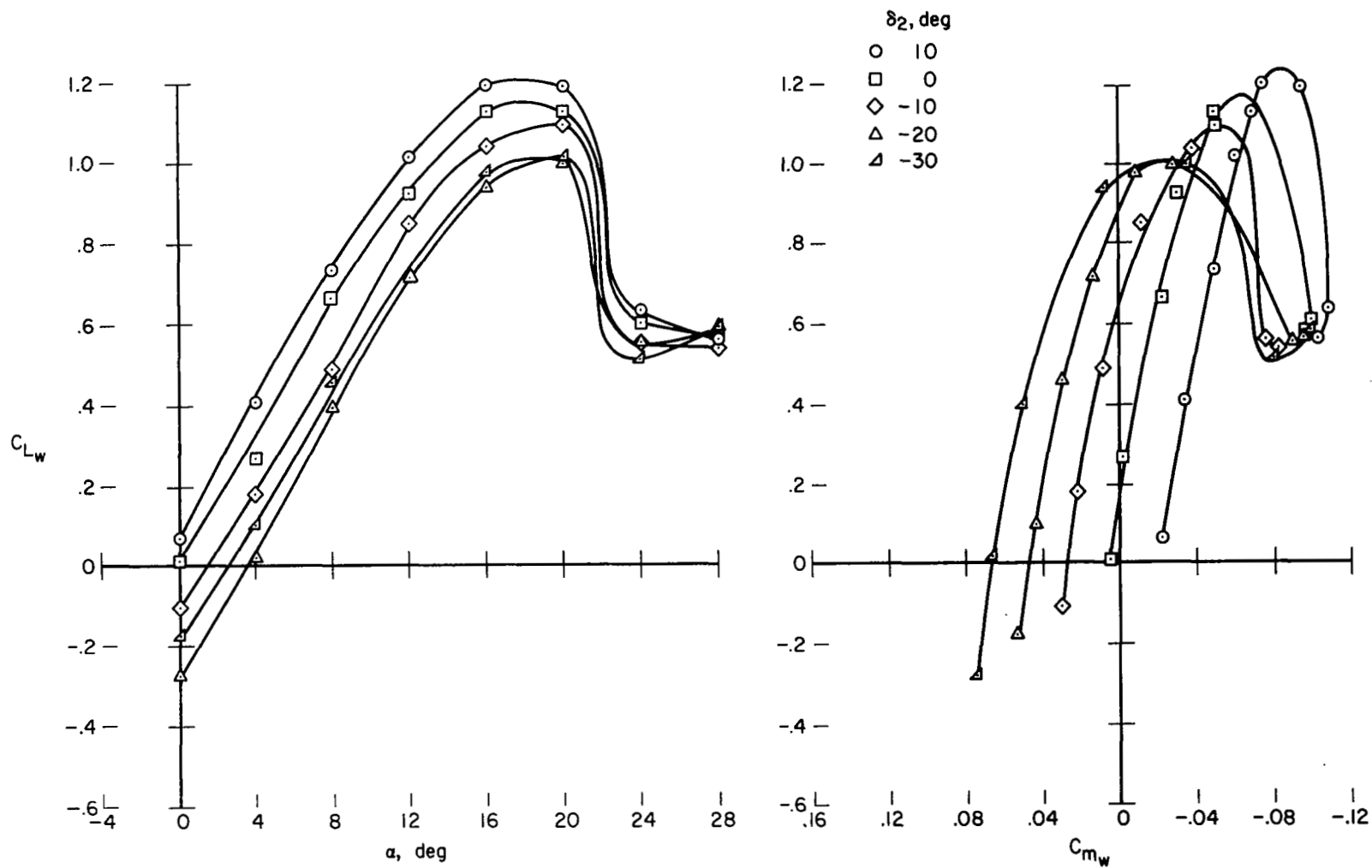
(c) Pivot location 21.60 percent; Re = 5.80×10⁵.

Figure 15.- Continued.
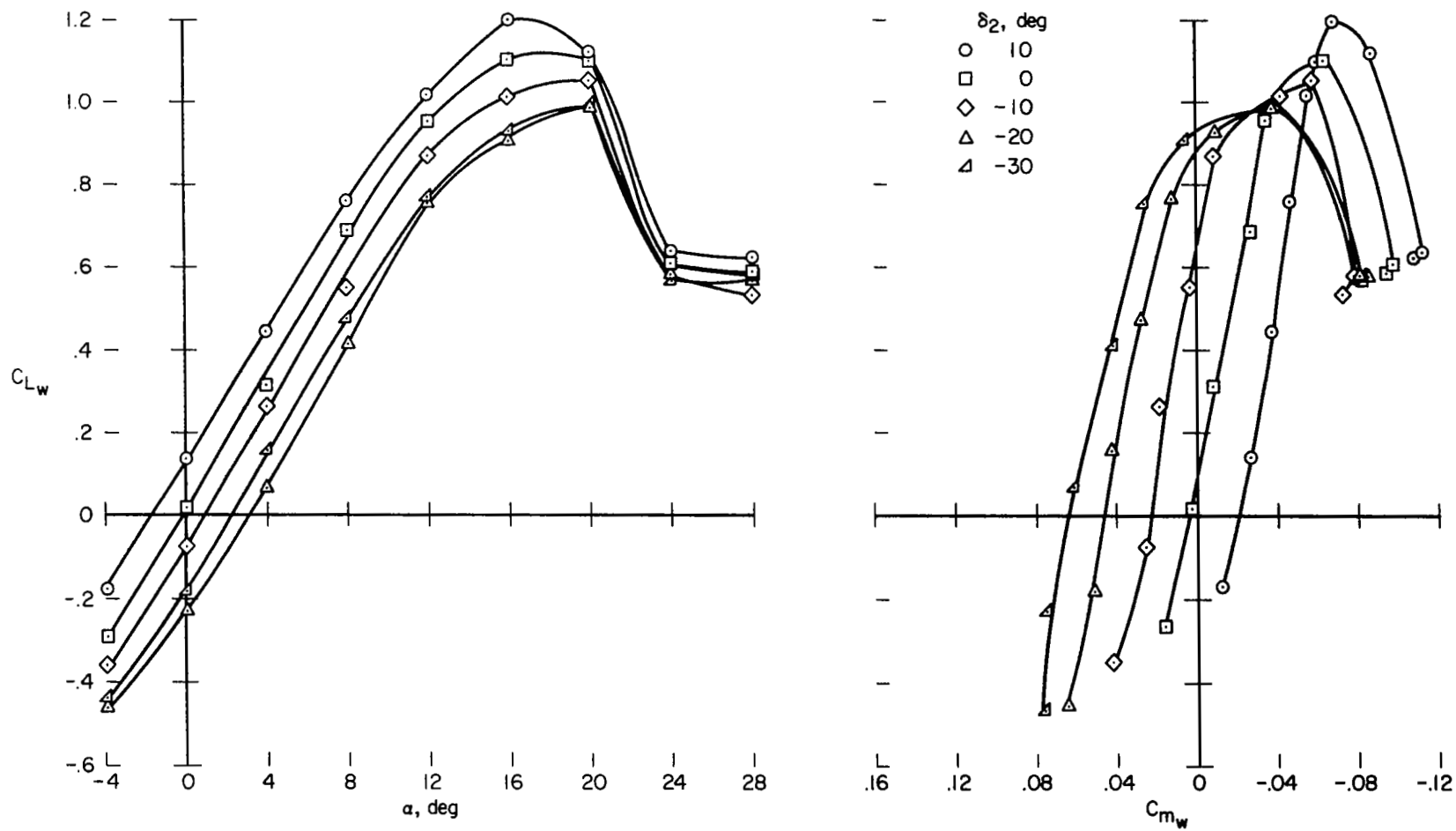
(d) Pivot location 21.60 percent; Re = 8.2×10⁵ .

Figure 15.- Concluded.
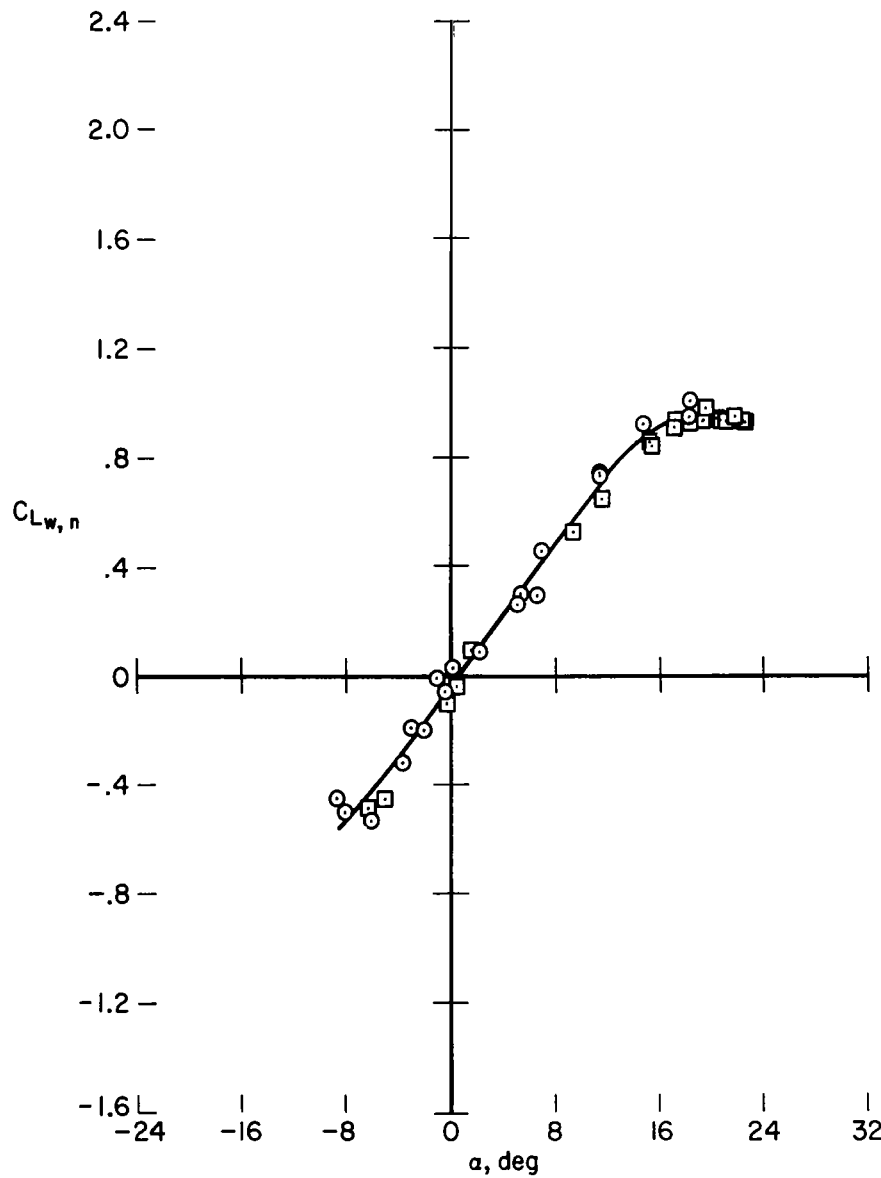
(a) Pivot location 19.8 percent.
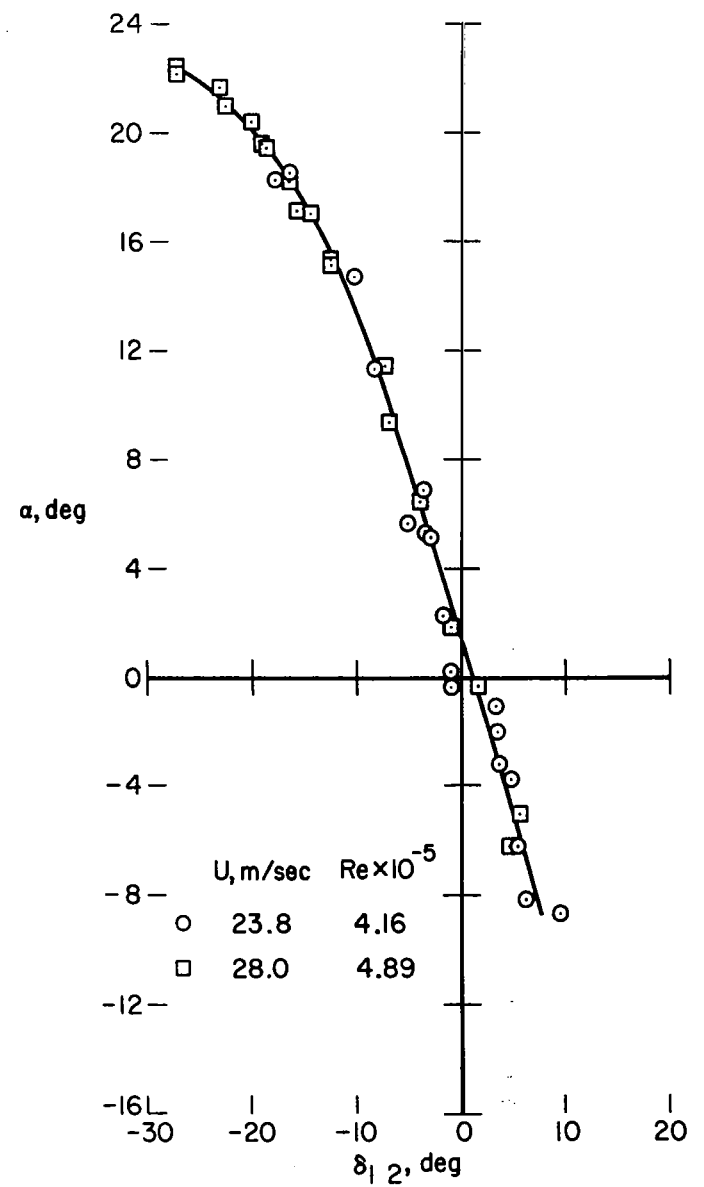
Figure 16.- Wing and nacelle lift coefficient and wing floating response; dynamic wing; propeller off; $\delta_3 = 0°$.
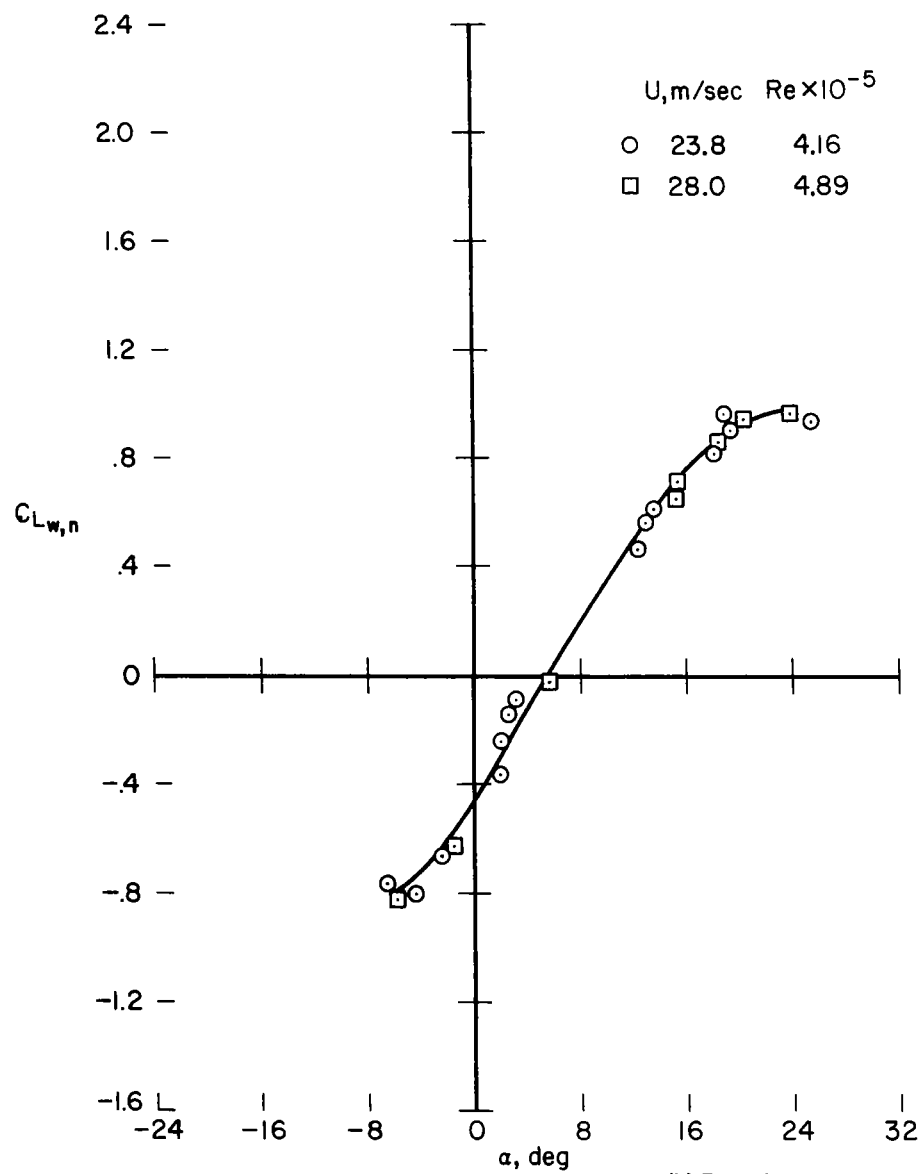
(b) Pivot location 21.6 percent.
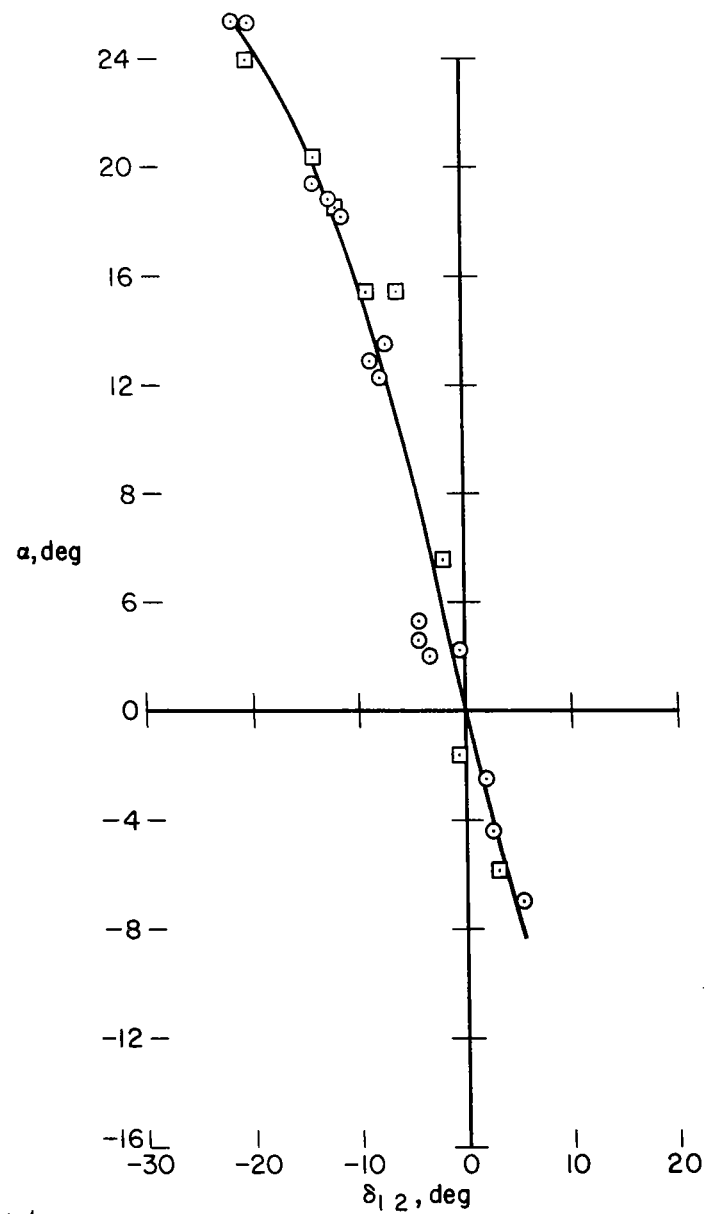
Figure 16.- Concluded.
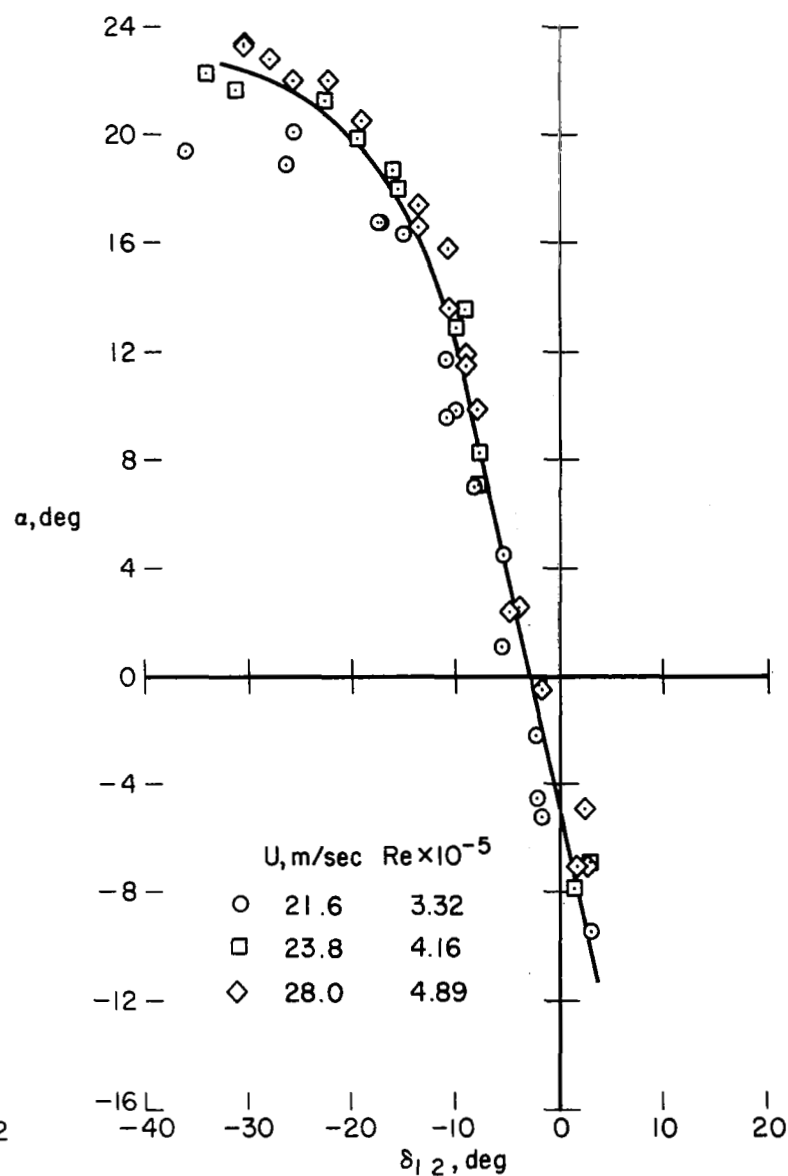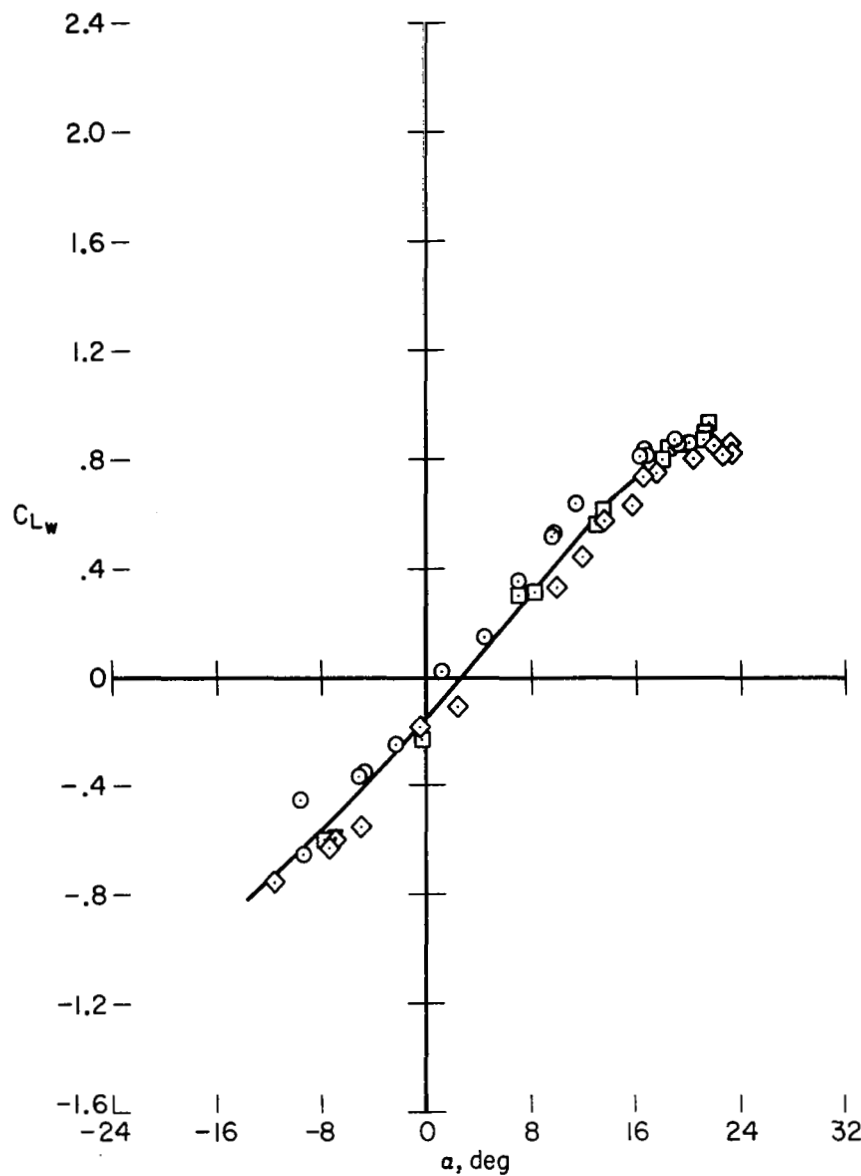
(a) Pivot location 19.8 percent.

Figure 17.- Wing lift coefficient and wing floating response; dynamic wing; propeller off; $\delta_3 = 0°$; nacelle removed.

U, m/sec	Re×10^{-5}
○ 21.6	3.32
□ 23.8	4.16
◇ 28.0	4.89
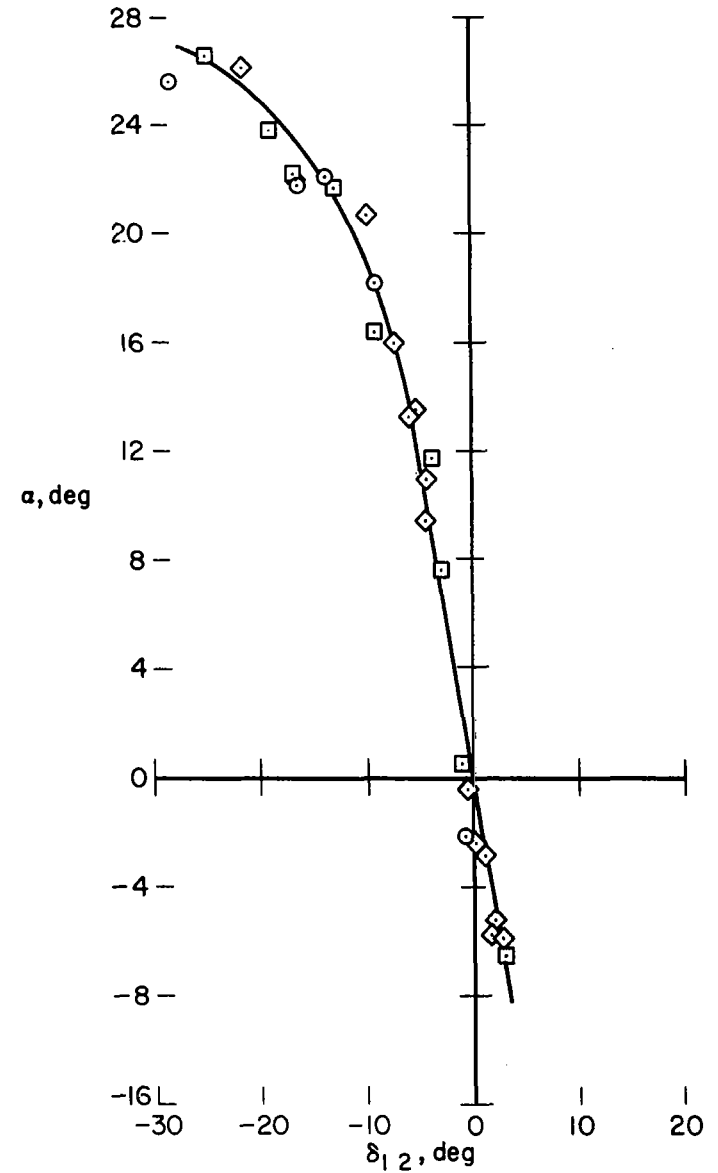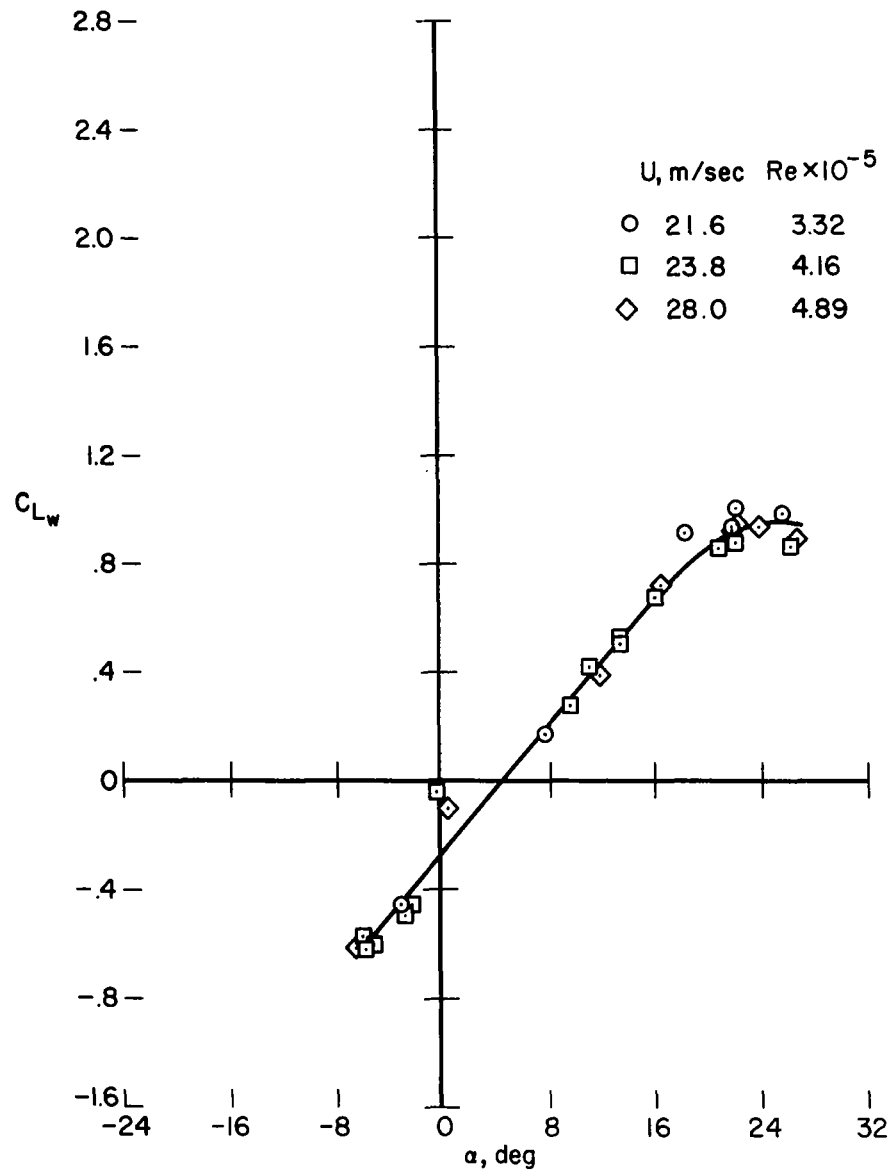
(b) Pivot location 21.6 percent.
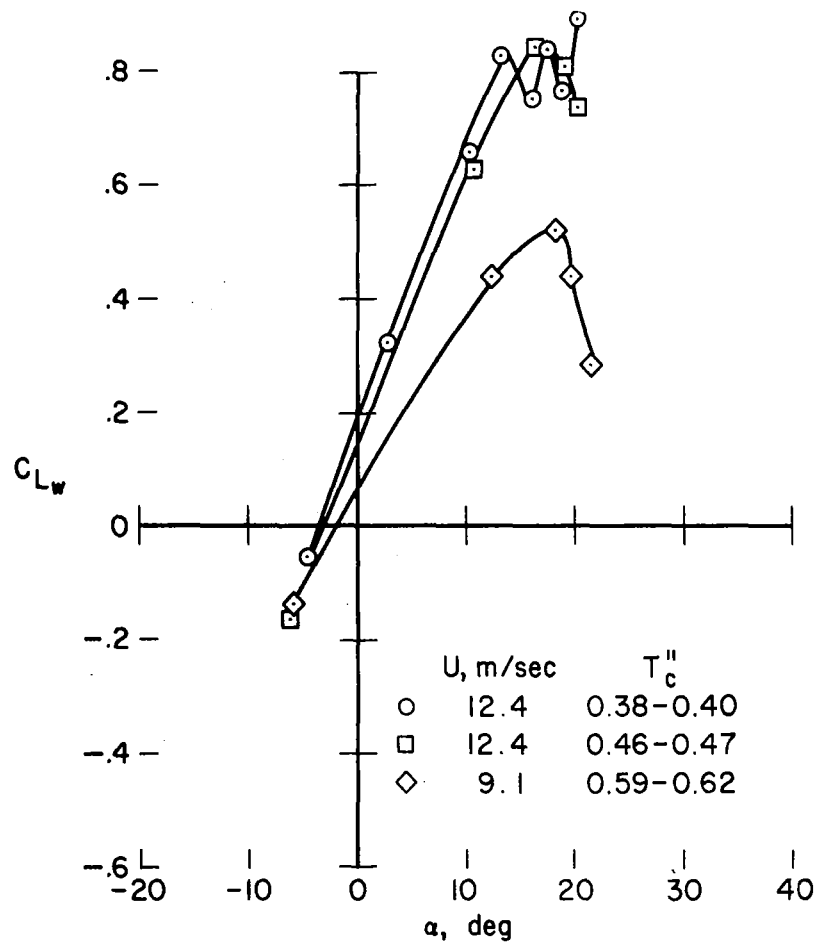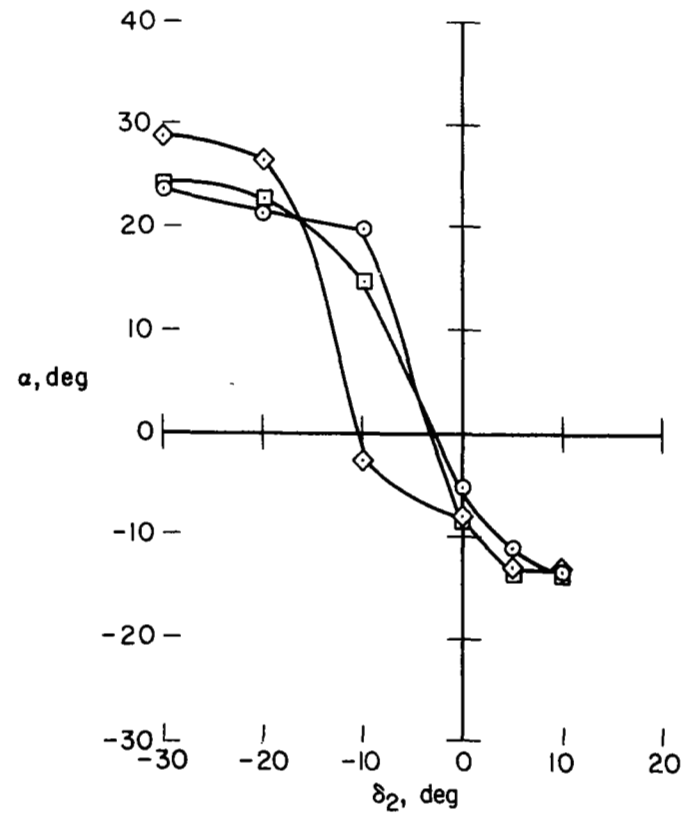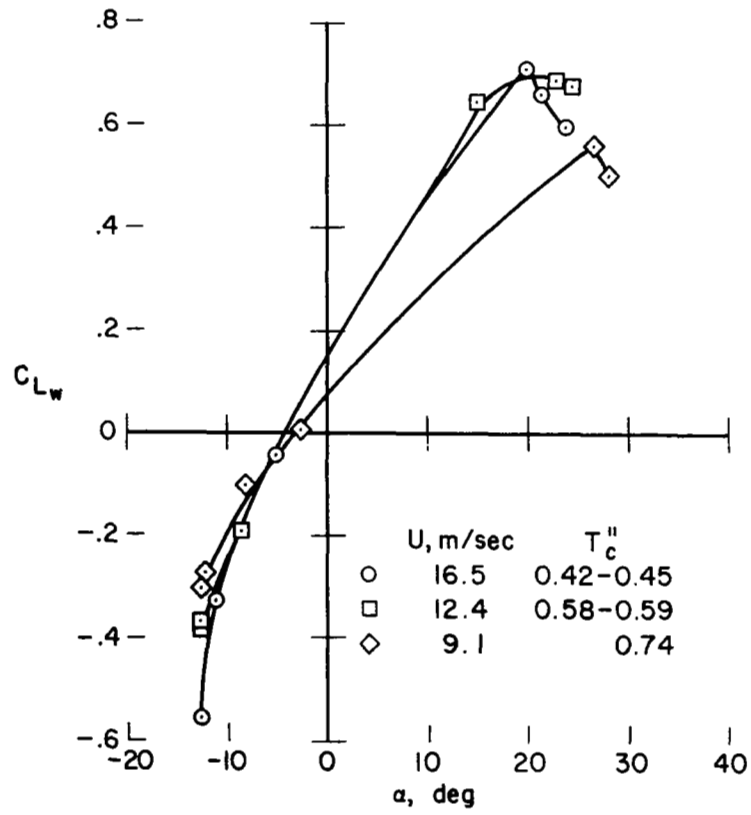
Figure 17.- Concluded.
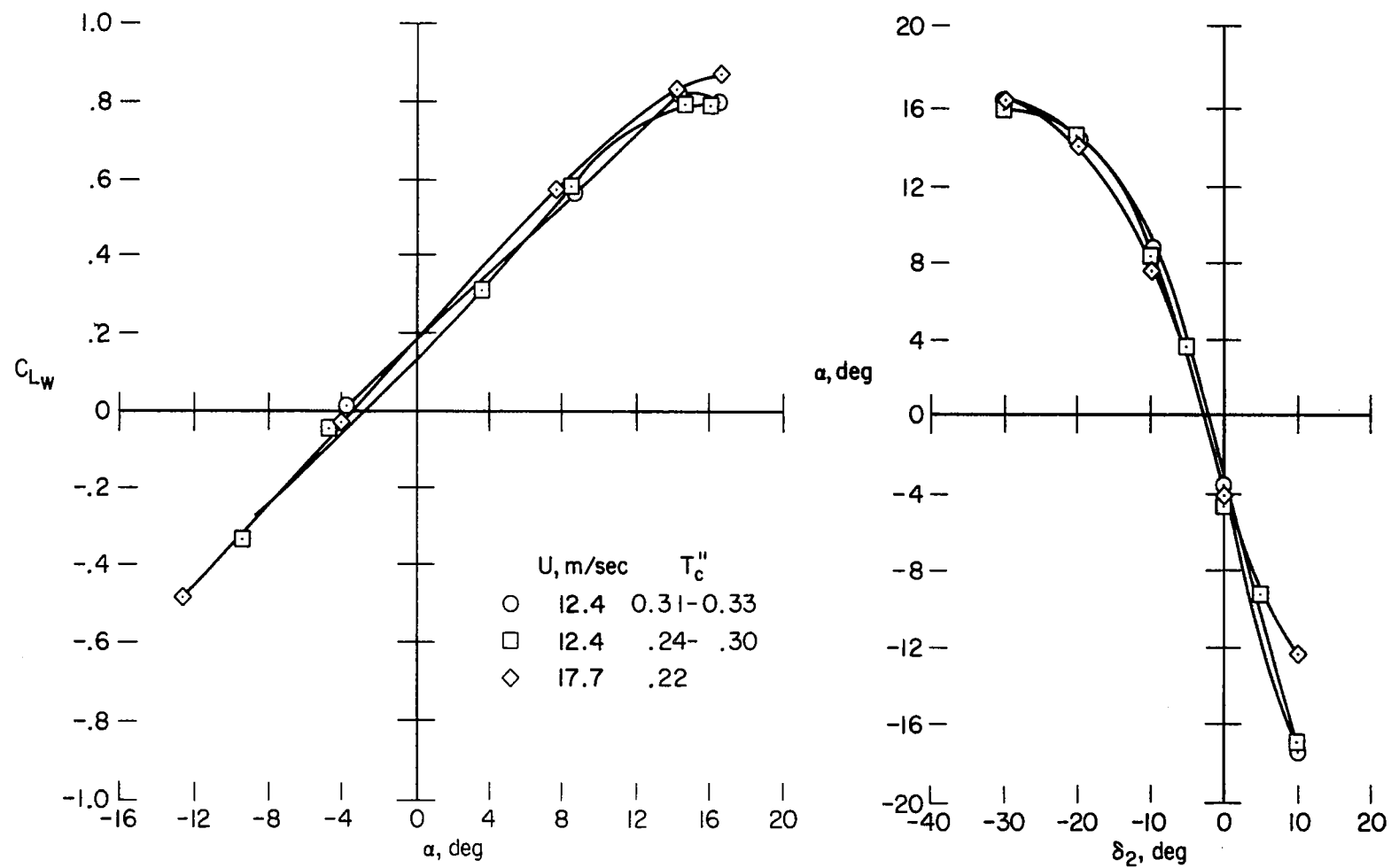
(a) $\alpha_p = 0°$

Figure 18.- Lift coefficient and floating response; static wing; pivot location 21.6 percent; power on; $\delta_{13} = 0°$.

C_{L_W}

α, deg

δ_2, deg

U, m/sec	T_c''
O 9.1	0.65
□ 12.4	.49-0.50
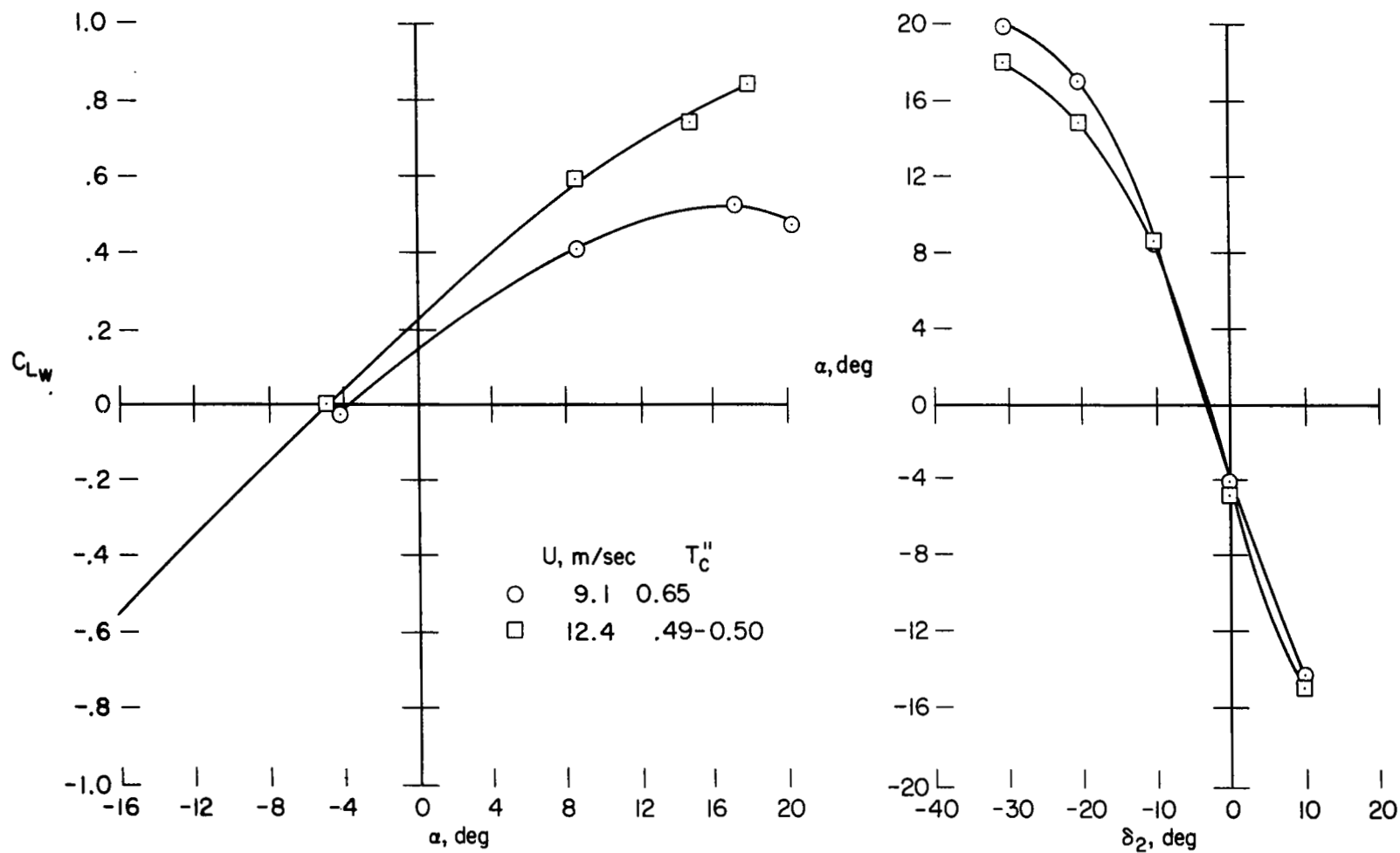
(b) $\alpha_p = 30°$

Figure 18.- Continued.
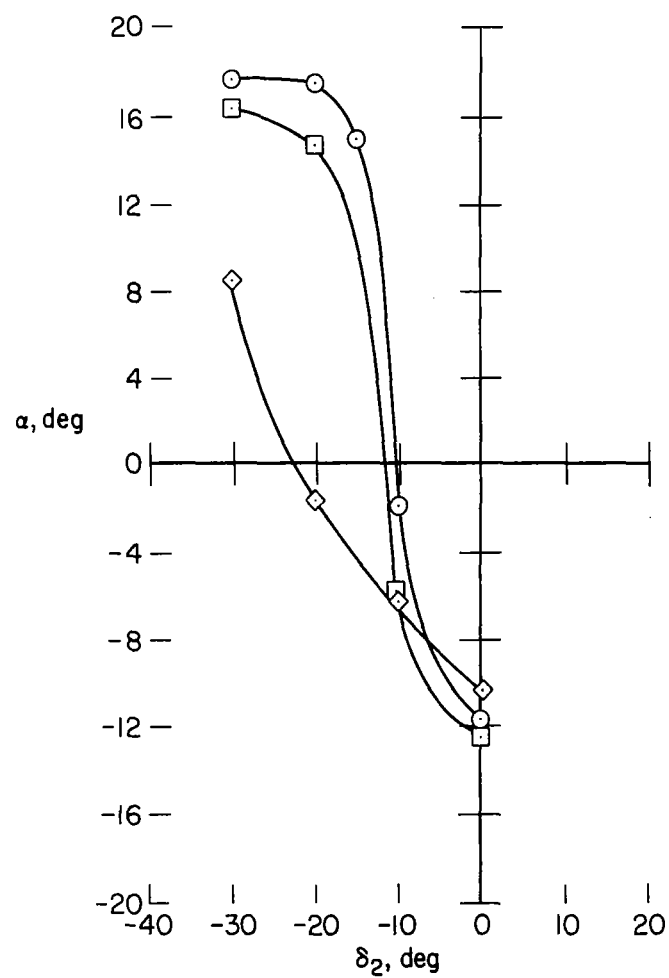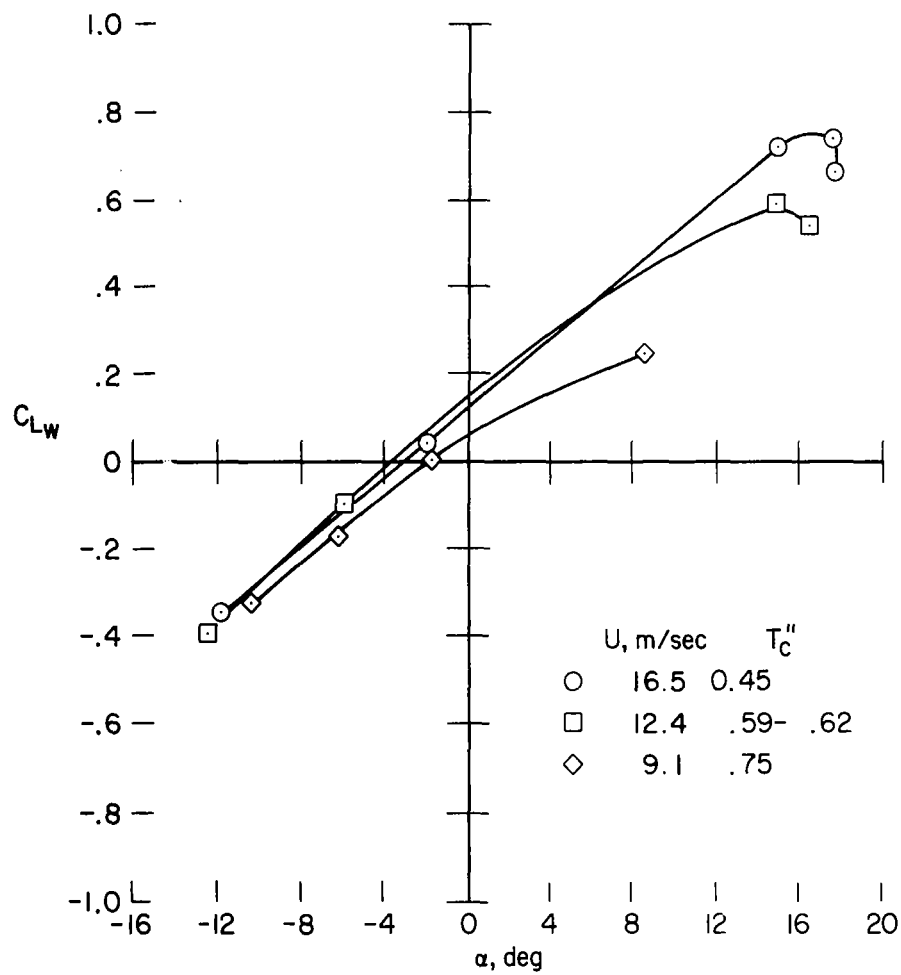
(c) $\alpha_p = 60°$

Figure 18.- Concluded.

$$C_{L_w}$$

$$\alpha, \text{ deg}$$

U, m/sec	T_c''
○ 12.4	0.23-0.25
□ 12.4	0.30-0.34

$\alpha, \text{ deg}$

$\delta_2, \text{ deg}$
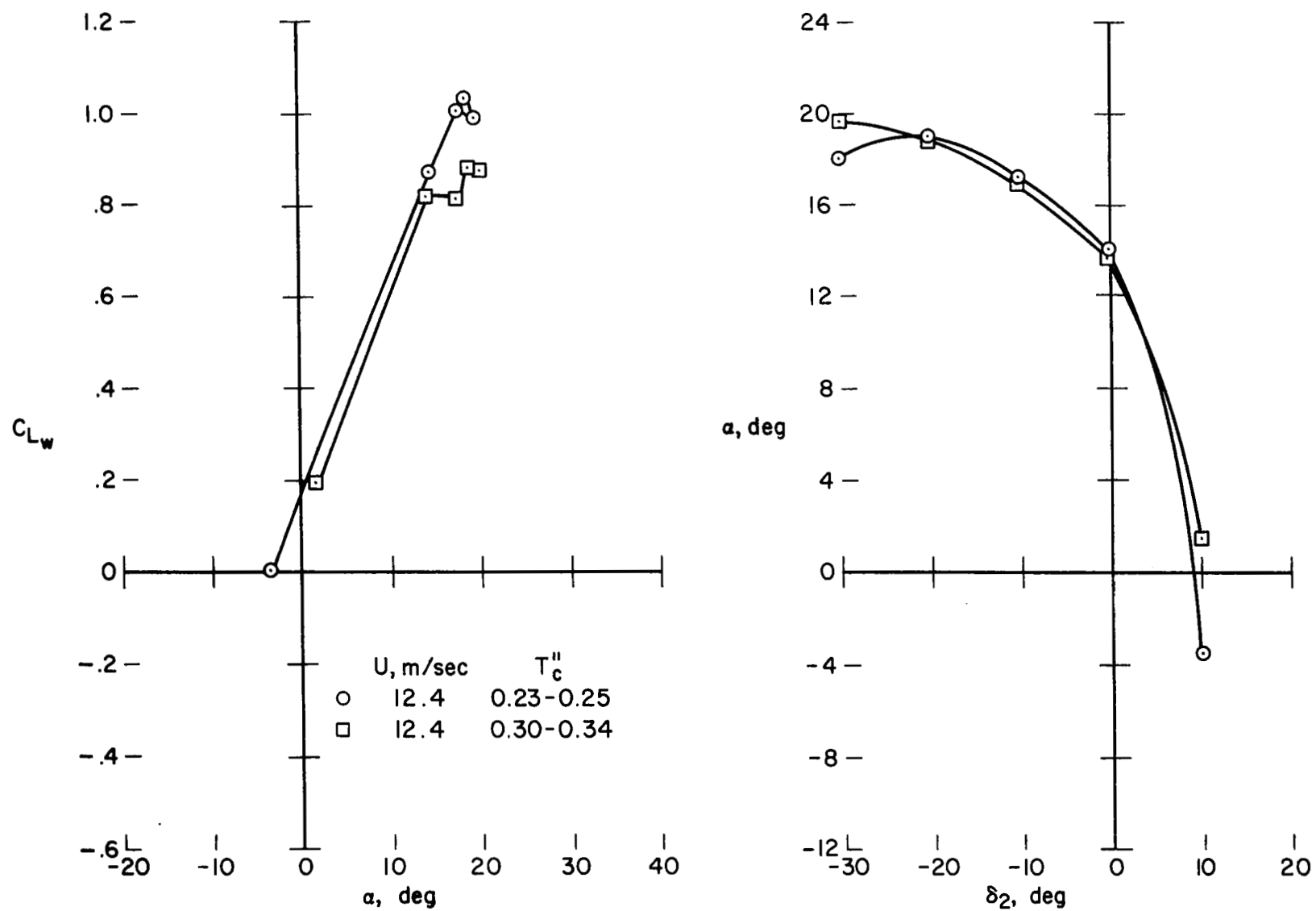
(a) $\alpha_p = 0°$

Figure 19.- Lift coefficient and floating response; static wing; pivot location 22.74 percent; power on; $\delta_{13} = 0°$.
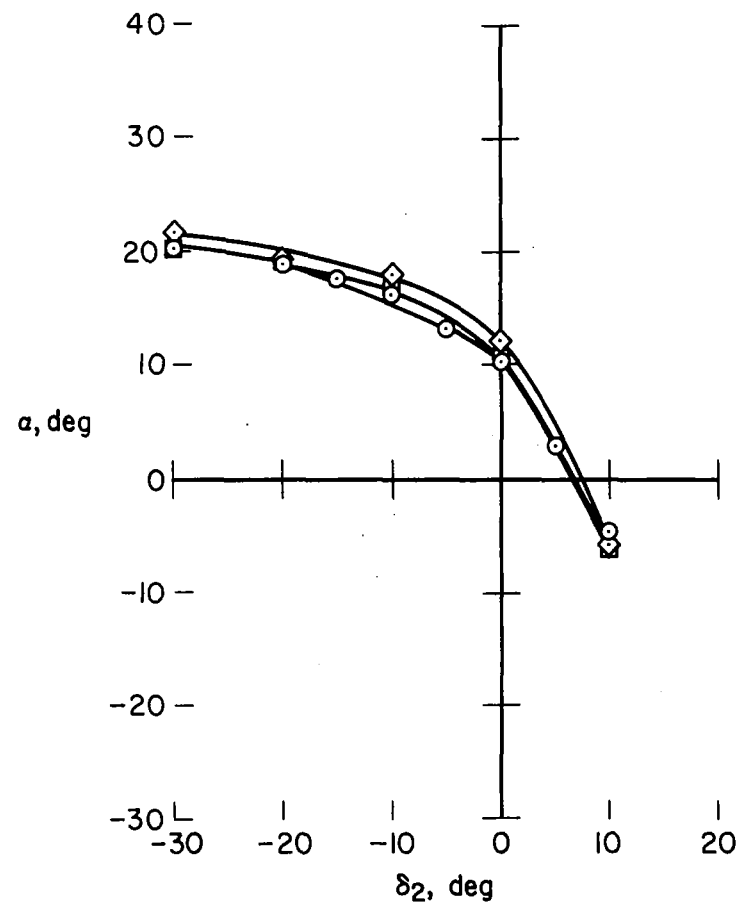
(b) $\alpha_p = 30°$

Figure 19.- Continued.

(c) $\alpha_p = 60°$

Figure 19.- Concluded.
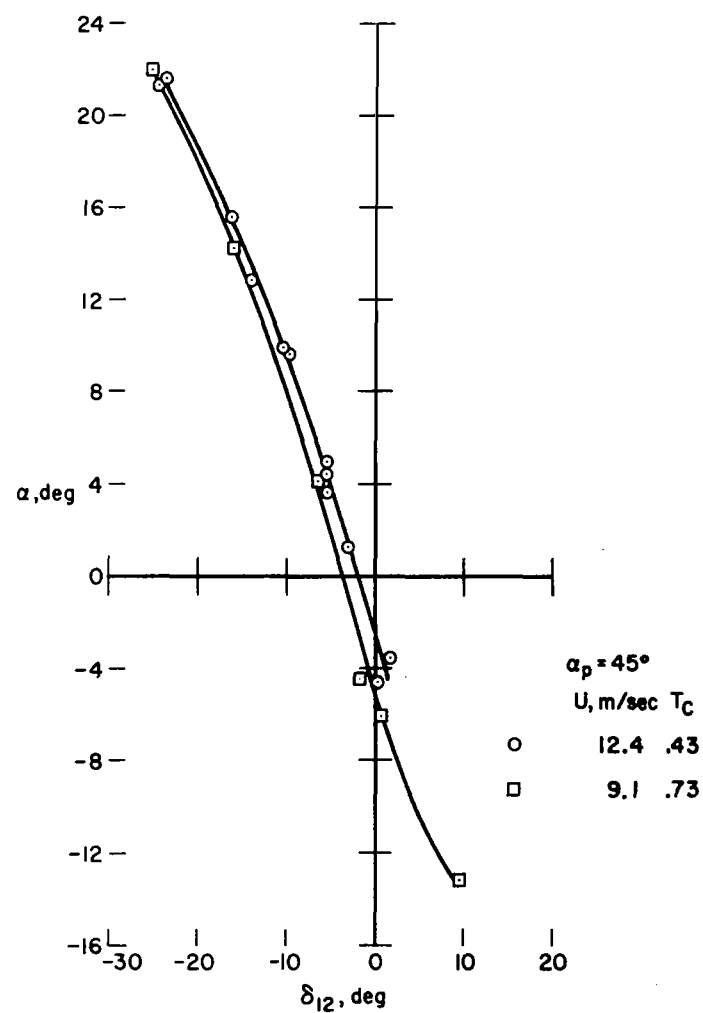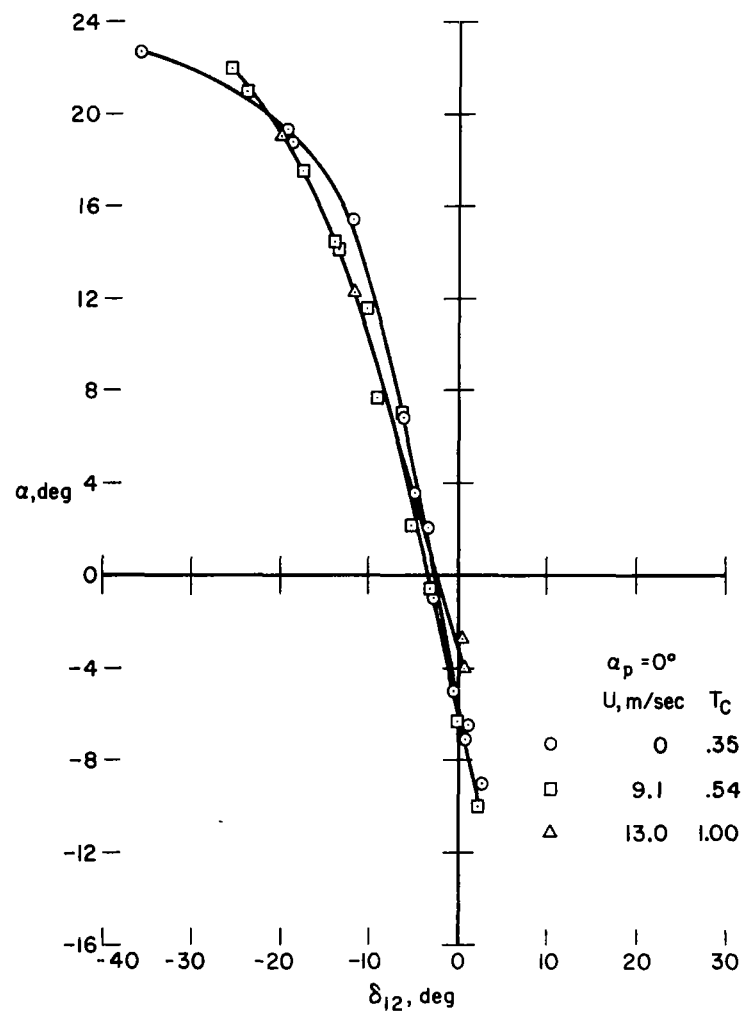
Figure 20.- Wing floating response; dynamic wing; power on; pivot location 19.8 percent; $\delta_3 = 0°$.

REFERENCES

1. Porter, Richard F.; and Brown, Joe H., Jr.: Evaluation of the Gust-Alleviation Characteristics and Handling Qualities of a Free-Wing Aircraft. NASA CR 1523, 1970.

2. Rainey, A. Gerald: Measurements of Aerodynamic Forces for Various Mean Angles of Attack on an Airfoil Oscillating in Pitch and on Two Finite-Span Wings Oscillating in Bending With Emphasis on Damping in the Stall. NACA TN 3643, 1956.

3. Liiva, Jan; Davenport, Franklyn J.; Gray, Lewis; and Walton, Ivor C.: Two-Dimensional Tests of Airfoils Oscillating Near Stall. Vol. 1: Summary and Evaluation of Results. USAAVLABS Tech. Rep. 68—13A, 1968.

4. Strand, T.; and Levinsky, E. S.: Wind-Tunnel Tests of a Free-Wing Tilt-Propeller V/STOL Airplane Model. Air Force Flight Dynamics Laboratory, Tech. Rep. AFFDL—TR—69—80, 1969.

5. Seckel, Edward: Stability and Control of Airplanes and Helicopters. Academic Press, Inc., 1964.

6. Bisplinghoff, Raymond L.; Ashley, Holt; and Halfman, Robert L.: Aeroelasticity. Addison-Wesley Pub. Co., Inc., Cambridge, Mass., 1955.